Please cite this article in press as: Saitsu et al., Mutations in *POLR3A* and *POLR3B* Encoding RNA Polymerase III Subunits Cause an Autosomal-Recessive Hypomyelinating Leukoencephalopathy, The American Journal of Human Genetics (2011), doi:10.1016/j.ajhg.2011.10.003

Table 1. Clinical Features of the Individuals

Clinical Features	Individual 1	Individual 2	Individual 3	Individual 4
Genes	*POLR3B*	*POLR3B*	*POLR3B*	*POLR3A*
Mutations, DNA	c.1857-2A>C, c.2303G>A	c.1857-2A>C, c.2303G>A	c.1648C>T, c.2778C>G	c.2690T>A, c.3013C>T
Mutations, protein	p.Asn620_Lys652del, p.Arg768His	p.Asn620_Lys652del, p.Arg768His	p.Arg550X, p.Asp926Glu	p.Ile897Asn, p.Arg1005Cys
Gender	M	F	F	M
Current age (years)	27	30	16	17
Intellectual disability	mild	mild	moderate	mild
Cognitive regression	–	–	–	–
Seizures	–	–	–	–
Initial motor development	normal	normal	normal	normal
Age of onset (years)	3	3	2	4
Motor deterioration	–	–	–	+
Wheelchair use	–	–	–	+
Optic atrophy	–	–	–	–
Myopia	+	+	–	+
Nystagmus	+	+	–	–
Abnormal pursuit	+	+	+	–
Vertical gaze limitation	+	+	+	–
Dysphagia	–	–	+	–
Hypersalivation	–	–	–	–
Cerebellar signs	+	+	+	+
Tremor	–	+	+	+
Babinski refex	–	–	–	–
Spasticity	–	–	mild	–
Peripheral nerve involvement	–	–	–	–
Nerve biopsy	NA	NA	NA	NA
Hypodontia	–	–	–	–
Hypogonadism	+	+	–	–

NA is an abbreviation for not available.

detected with NextGENe. Called SNVs were annotated with SeattleSeq Annotation.

We adopted a prioritization scheme to identify the pathogenic mutation in each individual, similar to the approach taken by recent studies (Table S2).[8–10] First, we excluded the variants registered in the dbSNP131 or 1000 Genome Project from all the detected variants. Then, SNVs commonly detected by MAQ and NextGENe analyses were selected as highly confident variants; 364 to 374 SNVs of nonsynonymous (NS) or canonical splice-site (SP) changes, along with 113 to 124 small insertions or deletions (indels), were identified per individual. We also excluded variants found in our 55 in-house exomes, which are derived from 12 healthy individuals and 43 individuals with unrelated diseases, reducing the number of candidate variants to ~250 per individual. Assuming that HCAHC is an autosomal-recessive disorder based on two affected individuals in one pedigree (individuals 1 and 2), we focused on rare heterozygous variants that are not registered in the dbSNP or in our in-house 55 exomes.

We surveyed all genes in each individual for two or more NS, SP, or indel variants. We found three to eight candidate genes per individual (Table S2). Among them, only *POLR3B* encoding RPC2, the second largest subunit of RNA Polymerase III (Pol III), was common in two individuals (individuals 1 and 3). The inheritance of the variants in *POLR3B* (transcript variant 1, NM_018082.5) was examined by Sanger sequencing. In individual 1, we confirmed that a canonical splice-site mutation (c.1857-2A>C [p.Asn620_Lys652del]), 2 bp upstream of exon 18, was

Please cite this article in press as: Saitsu et al., Mutations in *POLR3A* and *POLR3B* Encoding RNA Polymerase III Subunits Cause an Autosomal-Recessive Hypomyelinating Leukoencephalopathy, The American Journal of Human Genetics (2011), doi:10.1016/j.ajhg.2011.10.003

inherited from his father, and that a missense mutation (c.2303G>A [p.Arg768His]) in exon 21 were inherited from his mother (Figure 1A). The two mutations were also present in an affected elder sister (individual 2) but not present in a healthy elder brother. In individual 3, we confirmed that a nonsense mutation (c.1648C>T [p.Arg550X]) in exon 16 was inherited from her father and that a missense mutation (c.2778C>G [p.Asp926Glu]) in exon 24 was inherited from her mother (Figure 1A). The two mutations were not present in a healthy younger brother. To examine the mutational effects of c.1857-2A>C and c.1648C>T, reverse transcription PCR and sequencing with total RNA extracted from lymphoblastoid cells derived from the individuals was performed as previously described.[11] We demonstrated that the c.1857-2A>C mutation caused deletion of exon 18 from the *POLR3B* mRNA (Figures 2A–2C), resulting in an in-frame 33 amino acid deletion (p.Asn620_Lys652del) from RPC2 (Figure 1B). In addition, the mutated transcript harboring the nonsense mutation (c.1648C>T) was found to be expressed at a much lower level compared with the wild-type transcript (Figure 2D). The expression level of the mutated transcript was increased after treatment with 30 μM cycloheximide (CHX),[11] which inhibits nonsense-mediated mRNA decay (NMD), indicating that the mutant transcript underwent NMD (Figure 2D). The two missense mutations (p.Arg768His and p.Asp926Glu) found in the three individuals occurred at evolutionary conserved amino acids (Figure 1B). Among the other candidate genes in individuals 1 and 3, *MSLN* (MIM 601051), encoding mesothelin isoform 1 preproprotein that is cleaved into megakaryocyte potentiating factor and mesothelin, is a potential candidate in the family of individual 1 as its homozygous variant segregated with the phenotype; however, it is expressed in epithelial mesotheliomas, and the mutation affects less conserved amino acid (Table S3). The other candidate genes' variants did not cosegregate with the phenotype. Thus, mutations in *POLR3B* are most likely to cause HCAHC in two families.

In individual 4, in whom no *POLR3B* mutations were found, there were six candidate genes for an autosomal-recessive model. Among them, *POLR3A* (MIM 614258, GenBank accession number NM_007055.3), harboring two missense mutations, appeared to be a primary candidate because it encodes the largest subunit of Pol III (RPC1) (Figure 1A and Table S2). By Sanger sequencing, we confirmed that a missense mutation (c.2690T>A [p.Ile897Asn]) in exon 20 was inherited from his father and that another missense mutation (c.3013C>T [p.Arg1005Cys]) in exon 23 was inherited from his mother (Figure 1A). The two mutations were not present in a healthy younger sister. The two missense mutations (p.Ile897Asn and p.Arg1005Cys) occurred at relatively conserved amino acids (Figure 1B). In total, we found four mutations in *POLR3B* and two mutations in *POLR3A*. Evaluation of the missense mutations by PolyPhen-2 program showed that three mutations (p.Arg768His,

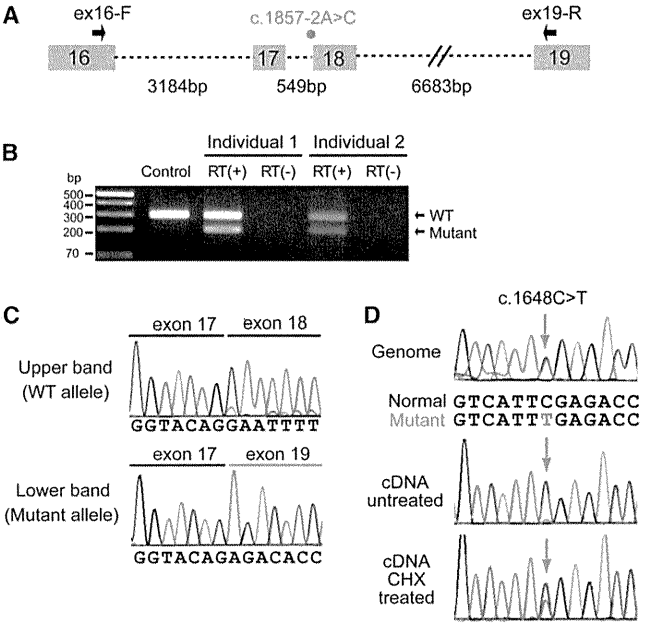

Figure 2. Effects of Splice-Site and Nonsense Mutations in *POLR3B*

(A) Schematic representation of the genomic structure of *POLR3B* from exon 16 to 19. Exons, introns, and primers are shown by boxes, dashed lines, and arrows, respectively. The mutation in intron 17 is depicted as a red dot.

(B) RT-PCR analysis of individuals 1 and 2 with c.1857-2A>C and a normal control. Two PCR products were detected from the individual's cDNA: the upper band is the wild-type (WT) transcript, and the lower band is the mutant. Only a single wild-type amplicon was detected in the control.

(C) Sequence of WT and mutant amplicons clearly showed exon 18 skipping in the mutant allele.

(D) Analysis of the c.1648C>T mutation. Sequence of PCR products amplified with genomic (upper), cDNA from untreated cells (middle), and cDNA from CHX treated cells (lower) as a template. Although untreated cells show extremely low levels of c.1648C>T mutant allele expression, cells treated to inhibit NMD show significantly increased levels of mutant allele expression.

p.Asp926Glu, and p.Ile897Asn) were probably damaging and that p.Arg1005Cys is tolerable. The c.2303G>A mutation (*POLR3B*) was found in one allele out of 540 Japanese control chromosomes. The remaining five mutations were not detected in 540 Japanese control chromosomes, indicating that the mutations are very rare in the Japanese population. Among the other candidate genes in individuals 4, *IGSF10*, a member of immunoglobulin superfamily, is a potential candidate because its variants segregated with the phenotype (Table S3); however, considering a close relationship between *POLR3A* and *POLR3B*, and the fact that *POLR3A* mutations have been recently reported in hypomyelinating leukodystrophy (see below),[12] *POLR3A* abnormality is the most plausible culprit for HCAHC in individual 4.

The structure of Pol III[13,14] and Pol II[15,16] is highly homologous, especially in the largest subunits. Thus, we extrapolated the mutations of RPC1 or RPC2 onto the structure of yeast Pol II (Protein Data Bank [PDB] accession number 3GTP)[17] (Figure 1C). RPB1 and RPB2 subunits of

Please cite this article in press as: Saitsu et al., Mutations in *POLR3A* and *POLR3B* Encoding RNA Polymerase III Subunits Cause an Autosomal-Recessive Hypomyelinating Leukoencephalopathy, The American Journal of Human Genetics (2011), doi:10.1016/j.ajhg.2011.10.003

yeast Pol II are homologous to RPC1 and RPC2 of Pol III, respectively. Asn620_Lys652 in RPC2 corresponds to Tyr679_Lys712 in RPB2. The deletion of Asn620_Lys652 (Tyr679_Lys712) would destroy a structural core of RPB2, leading to loss of RPB2 function. In addition, Arg768 (Arg852 in RPB2) interacts with the main-chain carbonyl group of Arg70 of the RPB12 subunit, and Asp926 (Asp1009 in RPB2) interacts with the side chain of Arg48 of the RPB10 subunit of Pol II (Figure 1D). Arg768His (Arg852His) and Asp926Glu (Asp1009Glu) substitutions are considered to disturb these subunit interactions, leading to dysfunction of the polymerase. Therefore, structural prediction suggests that the mutations in *POLR3B* (RPC2) could affect Pol III function. On the other hand, Ile897 and Arg1005 in RPC1 correspond to Val863 and Arg1036 in RPB1, respectively. Ile897 (Val863) has hydrophobic interactions with Leu170 and Pro176 of the RPB5 subunit and with Phe900 (Phe866) of the RPB1 subunit of Pol II (Figure 1E). Ile897Asn (Val863Asn) substitution is likely to disturb this interaction. Arg1005 (Arg1036) stabilizes interaction between RPB1 and RPB8 subunits (Figure 1F). The Arg1005Cys (Arg1036Cys) substitution appears to make this interaction unstable. Thus mutations in *POLR3A* are also predicted to affect Pol III function.

Clinical features of individuals with *POLR3A* or *POLR3B* mutations are presented in Table 1. MRI revealed high-intensity areas in the white matter in T2-weighted images, cerebellar atrophy, and a hypoplastic corpus callosum in all four individuals (Figure 3). Individuals 1 and 2 showed an extremely similar clinical course. They developed normally during their early infancy, i.e., walking unaided at 15 and 14 months, and uttering a few words at 12 and 13 months, respectively. After the age of 3, individual 1 presented with unstable walking and frequent stumbling and falling down, and individual 2 became poor at exercise. They both had severe myopia (corrected visual acuity of 0.7 and 0.5 at most, respectively). They graduated from elementary, junior high, and high schools with poor records, and the intelligence quotient (IQ) of individual 2 was 52 (WAIS-III). In individual 1, unstable walking was prominent at around 18 years, and he could not ride a bicycle because of ataxia; however, he could drive an automobile. Amenorrhea was noted in individual 2, and was successfully treated by hormone therapy. Individual 1 showed several signs of hypogonadism, including absence of underarm and mustache hair, thin pubic hair (Tanner II), and serum levels of testosterone, follicle stimulating hormone, and luteinizing hormone that were below normal for age 27. Neurological examination of both individuals revealed mild horizontal nystagmus, slowing of smooth-pursuit eye movement, and gaze limitation, especially in vertical gazing, hypotonia, mildly exaggerated deep-tendon reflex (patellar and Achilles tendon reflex) with negative Babinski reflex, and cerebellar signs and symptoms, including ataxic speech, wide-based ataxic gait, dysdiadochokinesis, and dysmetria. Clinical information for individual 3 has been reported previously.[6] Additional findings are as follows: slowing of smooth-pursuit eye movement, gaze limitation in vertical gazing, normal auditory brain responses (ABR), cerebral symptoms with mild spasticity, and intellectual disability (an IQ of 43 according to the WISC-III test), and no myopia but hypermetropic astigmatism. She showed no deterioration besides a mild dysphagia and walks herself to a school for the disabled. Individual 4 developed normally during his

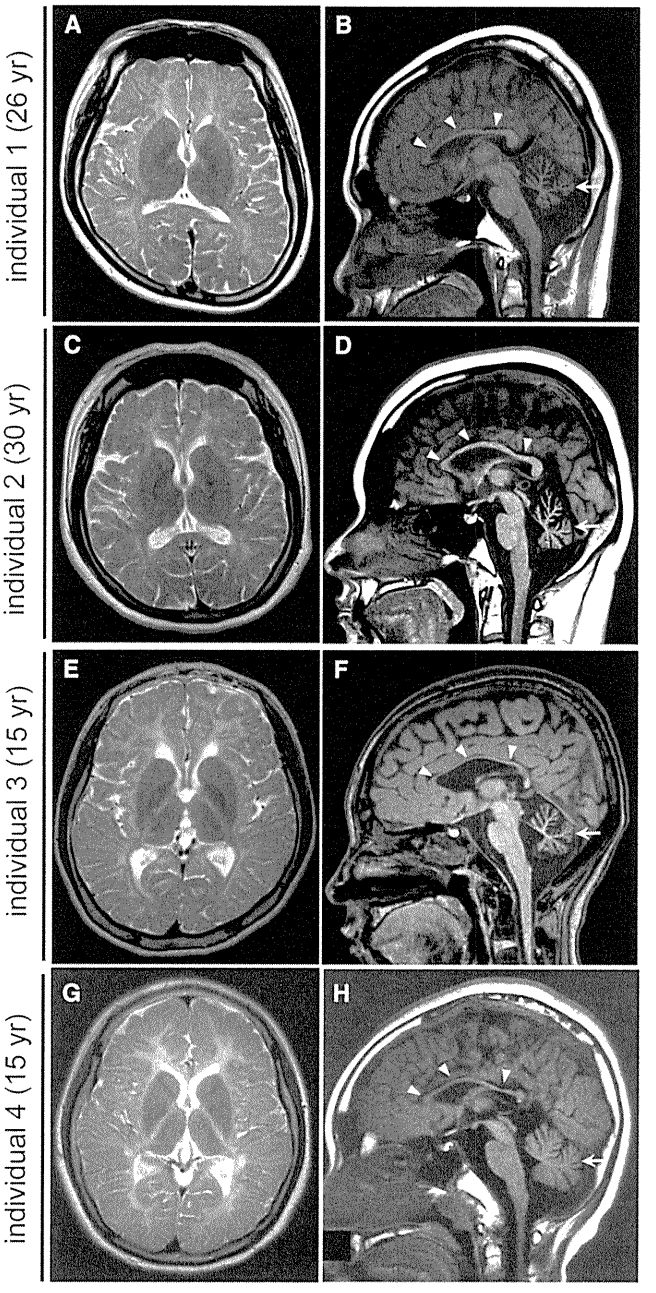

Figure 3. Brain MRI of Individuals with *POLR3B* and *POLR3A* Mutations

(A, C, E, and G) T2-weighted axial images through the basal ganglia. High-intensity areas in the white matter were observed in all individuals.

(B, D, F, and H) T1-weighted midline sagittal images. All the individuals showed hypoplastic corpus callosum (arrowheads) and atrophy of cerebellum (arrows).

Please cite this article in press as: Saitsu et al., Mutations in *POLR3A* and *POLR3B* Encoding RNA Polymerase III Subunits Cause an Autosomal-Recessive Hypomyelinating Leukoencephalopathy, The American Journal of Human Genetics (2011), doi:10.1016/j.ajhg.2011.10.003

early infancy, had normal head control at 3 months, was speaking a few words at 12 months, and was walking unaided at 14 months. His parents noted mild tremors around 4 years. He had normal stature, weight, and head circumference. Although he had severe myopia, his eye movement was smooth with no limitation or nystagmus. He had sensory neuronal deafness on the left side. He showed normal muscle tone and had no spasticity or rigidity. His tendon reflexes were slightly elevated with a negative Babinski reflex. Cerebellar signs were noted; expressive ataxic explosive speech, intension tremor, poor finger to nose test, dysdiadochokinesis, dysmetria, and wide-based ataxic gait. His intelligence quotient was 57 (according to the WISC-III test). His peripheral nerve conduction velocity was within the normal range and his ABR showed normal responses on the right side. He suffered motor deterioration around age 14 and became wheelchair bound.

In this study, we successfully identified compound heterozygous mutations in *POLR3A* and *POLR3B* in individuals with HCAHC. Very recently, Bernard et al.[12] reported that *POLR3A* mutations cause three overlapping leukodystrophies, including 4H syndrome, suggesting that HCAHC is, at least in part, within a wide clinical spectrum caused by *POLR3A* mutations. The p.Arg1005Cys mutation was shared between individual 9 in their report and our individual 4. All 19 individuals with *POLR3A* mutations showed progressive upper motor neuron dysfunction and cognitive regression. In addition, individual 9 showed abnormal eye movement, hypodontia, and hypogonadism. None of these features were recognized in our individual 4; these differences further support phenotypic variability of *POLR3A* mutations.[12] Given the phenotypic similarities among 4H syndrome, HCAHC, and H-ABC, there is a possibility that H-ABC is also allelic and caused by recessive mutations in either *POLR3A* or *POLR3B*.

Pol III consists of 17 subunits and is involved in the transcription of small noncoding RNAs, such as 5S ribosomal RNA (rRNA), U6 small nuclear RNA (snRNA), 7SL RNA, RNase P, RNase MRP, short interspersed nuclear elements (SINEs), and all transfer RNAs (tRNAs). Pol III-transcribed genes are classified into three types based on promoter elements and transcription factors. 5S rRNA is a solo type I gene. Type II genes include tRNA, 7SL RNA, and SINEs. Type III genes include U6 snRNA, RNase P, and RNase MRP.[18–20] The Pol III system is important for cell growth in yeast, and its transcription is tightly regulated during the cell cycle.[20] In zebrafish, *polr3b* mutant larvae that have a deletion of 41 conserved amino acids (Δ239-279) from the Rpc2 protein showed a proliferation deficit in multiple tissues, including intestine, endocrine pancreas, liver, retina and terminal branchial arches.[21] In the mutants, the expression levels of tRNA were significantly reduced, whereas the level of 5S rRNA expression was not changed, suggesting that this *polr3b* mutation can differentially affect Pol III target promoters.[21] RPC2 contributes to the catalytic activity of the polymerase and forms the active center of the polymerase together with the largest subunit, RPC1.[22] Thus, it is reasonable to consider that mutations in *POLR3A* and *POLR3B* cause overlapping phenotypes. Indeed, three individuals with *POLR3B* mutations showed diffuse cerebral hypomyelination, atrophy of the cerebellum and corpus callosum, and abnormal eye movements that overlap with *POLR3A* abnormalities.[12] Furthermore, two out of three individuals showed hypogonadism, suggesting a common pathological mechanism between *POLR3A* and *POLR3B* mutations. In the zebrafish *polr3b* mutants there were no defects of the central nervous system other than a reduced size of the retina, probably reflecting species differences; however, the reduced level of tRNA in the *polr3b* mutants raises the possibility that defects of tRNA transcription by Pol III could be a common pathological mechanism underlying *POLR3A* and *POLR3B* mutations. Supporting this idea, mutations in two genes involved in aminoacylation activity of tRNA synthetase cause defects of myelination in central nervous system: *DARS2* (MIM 610956) and *AIMP* (MIM 603605).[23,24] In addition, mutations in four genes encoding aminoacyl-tRNA synthetase cause Charcot-Marie-Tooth disease (MIM 613641, 613287, 601472, and 608323), resulting from demyelination of peripheral nerve axons: *KARS* (MIM 601421), *GARS* (MIM 600287), *YARS* (MIM 603623), and *AARS* (MIM 601065).[25–28] Thus, it is very likely that regulation of tRNA expression is essential for development and maintenance of myelination in both central and peripheral nervous systems.

An interesting clinical feature of *POLR3B* mutations is the absence of motor deterioration. All three individuals with *POLR3B* mutations could walk without support at ages 16, 27, and 30, whereas individual 3 with *POLR3A* mutations had motor deterioration around age 14. Bernard et al.[12] also reported progressive upper motor neuron dysfunction and cognitive regression in individuals with *POLR3A* mutations. Thus, there is a possibility that phenotypes caused by *POLR3A* mutations could be more severe and progressive than *POLR3B* mutant phenotypes. Identification of a greater number of cases with *POLR3B* mutations is required to confirm this hypothesis.

In conclusion, our data, together with that of a previous report,[12] demonstrate that mutations in Pol III subunits cause overlapping autosomal-recessive hypomyelinating disorders. Establishment of an animal model will facilitate our understanding of the pathophysiology of the multiple defects caused by Pol III mutations.

Supplemental Data

Supplemental Data include three tables and can be found with this article online at http://www.cell.com/AJHG/.

Acknowledgments

We would like to thank all the individuals and their families for their participation in this study. This work was supported by

Please cite this article in press as: Saitsu et al., Mutations in *POLR3A* and *POLR3B* Encoding RNA Polymerase III Subunits Cause an Autosomal-Recessive Hypomyelinating Leukoencephalopathy, The American Journal of Human Genetics (2011), doi:10.1016/j.ajhg.2011.10.003

research grants from the Ministry of Health, Labour, and Welfare (H.S., H.O., M.S., J.T., N. Miyake, K.I. and N. Matsumoto), the Japan Science and Technology Agency (N. Matsumoto), a Grant-in-Aid for Scientific Research on Innovative Areas (Foundation of Synapse and Neurocircuit Pathology) from the Ministry of Education, Culture, Sports, Science and Technology of Japan (N. Matsumoto), a Grant-in-Aid for Scientific Research from Japan Society for the Promotion of Science (H.O., N. Matsumoto), a Grant-in-Aid for Young Scientist from Japan Society for the Promotion of Science (H.S.). This work has been done at Advanced Medical Research Center, Yokohama City University.

Received: August 31, 2011
Revised: October 5, 2011
Accepted: October 10, 2011
Published online: October 27, 2011

Web Resources

The URLs for data presented herein are as follows:

ClustalW, http://www.genome.jp/tools/clustalw/
dbSNP, http://www.ncbi.nlm.nih.gov/projects/SNP/
Ensembl, http://uswest.ensembl.org/index.html
GenBank, http://www.ncbi.nlm.nih.gov/Genbank/
Online Mendelian Inheritance in Man, http://www.omim.org
PolyPhen-2, http://genetics.bwh.harvard.edu/pph2/
Protein Data Bank, http://www.pdb.org/pdb/home/home.do
PyMOL, http://www.pymol.org/
SeattleSeq Annotation, http://gvs.gs.washington.edu/SeattleSeqAnnotation/

References

1. Schiffmann, R., and van der Knaap, M.S. (2009). Invited article: an MRI-based approach to the diagnosis of white matter disorders. Neurology *72*, 750–759.
2. Timmons, M., Tsokos, M., Asab, M.A., Seminara, S.B., Zirzow, G.C., Kaneski, C.R., Heiss, J.D., van der Knaap, M.S., Vanier, M.T., Schiffmann, R., and Wong, K. (2006). Peripheral and central hypomyelination with hypogonadotropic hypogonadism and hypodontia. Neurology *67*, 2066–2069.
3. Wolf, N.I., Harting, I., Boltshauser, E., Wiegand, G., Koch, M.J., Schmitt-Mechelke, T., Martin, E., Zschocke, J., Uhlenberg, B., Hoffmann, G.F., et al. (2005). Leukoencephalopathy with ataxia, hypodontia, and hypomyelination. Neurology *64*, 1461–1464.
4. Wolf, N.I., Harting, I., Innes, A.M., Patzer, S., Zeitler, P., Schneider, A., Wolff, A., Baier, K., Zschocke, J., Ebinger, F., et al. (2007). Ataxia, delayed dentition and hypomyelination: a novel leukoencephalopathy. Neuropediatrics *38*, 64–70.
5. van der Knaap, M.S., Naidu, S., Pouwels, P.J., Bonavita, S., van Coster, R., Lagae, L., Sperner, J., Surtees, R., Schiffmann, R., and Valk, J. (2002). New syndrome characterized by hypomyelination with atrophy of the basal ganglia and cerebellum. AJNR Am. J. Neuroradiol. *23*, 1466–1474.
6. Sasaki, M., Takanashi, J., Tada, H., Sakuma, H., Furushima, W., and Sato, N. (2009). Diffuse cerebral hypomyelination with cerebellar atrophy and hypoplasia of the corpus callosum. Brain Dev. *31*, 582–587.
7. Li, H., Ruan, J., and Durbin, R. (2008). Mapping short DNA sequencing reads and calling variants using mapping quality scores. Genome Res. *18*, 1851–1858.
8. Doi, H., Yoshida, K., Yasuda, T., Fukuda, M., Fukuda, Y., Morita, H., Ikeda, S., Kato, R., Tsurusaki, Y., Miyake, N., et al. (2011). Exome sequencing reveals a homozygous *SYT14* mutation in adult-onset, autosomal-recessive spinocerebellar ataxia with psychomotor retardation. Am. J. Hum. Genet. *89*, 320–327.
9. Pierce, S.B., Walsh, T., Chisholm, K.M., Lee, M.K., Thornton, A.M., Fiumara, A., Opitz, J.M., Levy-Lahad, E., Klevit, R.E., and King, M.C. (2010). Mutations in the DBP-deficiency protein HSD17B4 cause ovarian dysgenesis, hearing loss, and ataxia of Perrault Syndrome. Am. J. Hum. Genet. *87*, 282–288.
10. Gilissen, C., Arts, H.H., Hoischen, A., Spruijt, L., Mans, D.A., Arts, P., van Lier, B., Steehouwer, M., van Reeuwijk, J., Kant, S.G., et al. (2010). Exome sequencing identifies *WDR35* variants involved in Sensenbrenner syndrome. Am. J. Hum. Genet. *87*, 418–423.
11. Saitsu, H., Kato, M., Okada, I., Orii, K.E., Higuchi, T., Hoshino, H., Kubota, M., Arai, H., Tagawa, T., Kimura, S., et al. (2010). *STXBP1* mutations in early infantile epileptic encephalopathy with suppression-burst pattern. Epilepsia *51*, 2397–2405.
12. Bernard, G., Chouery, E., Putorti, M.L., Tetreault, M., Takanohashi, A., Carosso, G., Clement, I., Boespflug-Tanguy, O., Rodriguez, D., Delague, V., et al. (2011). Mutations of *POLR3A* Encoding a Catalytic Subunit of RNA Polymerase Pol III Cause a Recessive Hypomyelinating Leukodystrophy. Am. J. Hum. Genet. *89*, 415–423.
13. Jasiak, A.J., Armache, K.J., Martens, B., Jansen, R.P., and Cramer, P. (2006). Structural biology of RNA polymerase III: subcomplex C17/25 X-ray structure and 11 subunit enzyme model. Mol. Cell *23*, 71–81.
14. Fernández-Tornero, C., Böttcher, B., Riva, M., Carles, C., Steuerwald, U., Ruigrok, R.W., Sentenac, A., Müller, C.W., and Schoehn, G. (2007). Insights into transcription initiation and termination from the electron microscopy structure of yeast RNA polymerase III. Mol. Cell *25*, 813–823.
15. Cramer, P., Bushnell, D.A., and Kornberg, R.D. (2001). Structural basis of transcription: RNA polymerase II at 2.8 angstrom resolution. Science *292*, 1863–1876.
16. Gnatt, A.L., Cramer, P., Fu, J., Bushnell, D.A., and Kornberg, R.D. (2001). Structural basis of transcription: an RNA polymerase II elongation complex at 3.3 A resolution. Science *292*, 1876–1882.
17. Wang, D., Bushnell, D.A., Huang, X., Westover, K.D., Levitt, M., and Kornberg, R.D. (2009). Structural basis of transcription: backtracked RNA polymerase II at 3.4 angstrom resolution. Science *324*, 1203–1206.
18. Oler, A.J., Alla, R.K., Roberts, D.N., Wong, A., Hollenhorst, P.C., Chandler, K.J., Cassiday, P.A., Nelson, C.A., Hagedorn, C.H., Graves, B.J., and Cairns, B.R. (2010). Human RNA polymerase III transcriptomes and relationships to Pol II promoter chromatin and enhancer-binding factors. Nat. Struct. Mol. Biol. *17*, 620–628.
19. Dieci, G., Fiorino, G., Castelnuovo, M., Teichmann, M., and Pagano, A. (2007). The expanding RNA polymerase III transcriptome. Trends Genet. *23*, 614–622.
20. Dumay-Odelot, H., Durrieu-Gaillard, S., Da Silva, D., Roeder, R.G., and Teichmann, M. (2010). Cell growth- and differentiation-dependent regulation of RNA polymerase III transcription. Cell Cycle *9*, 3687–3699.

21. Yee, N.S., Gong, W., Huang, Y., Lorent, K., Dolan, A.C., Maraia, R.J., and Pack, M. (2007). Mutation of RNA Pol III subunit *rpc2/polr3b* Leads to Deficiency of Subunit Rpc11 and disrupts zebrafish digestive development. PLoS Biol. *5*, e312.
22. Werner, M., Thuriaux, P., and Soutourina, J. (2009). Structure-function analysis of RNA polymerases I and III. Curr. Opin. Struct. Biol. *19*, 740–745.
23. Scheper, G.C., van der Klok, T., van Andel, R.J., van Berkel, C.G., Sissler, M., Smet, J., Muravina, T.I., Serkov, S.V., Uziel, G., Bugiani, M., et al. (2007). Mitochondrial aspartyl-tRNA synthetase deficiency causes leukoencephalopathy with brain stem and spinal cord involvement and lactate elevation. Nat. Genet. *39*, 534–539.
24. Feinstein, M., Markus, B., Noyman, I., Shalev, H., Flusser, H., Shelef, I., Liani-Leibson, K., Shorer, Z., Cohen, I., Khateeb, S., et al. (2010). Pelizaeus-Merzbacher-like disease caused by AIMP1/p43 homozygous mutation. Am. J. Hum. Genet. *87*, 820–828.
25. Latour, P., Thauvin-Robinet, C., Baudelet-Méry, C., Soichot, P., Cusin, V., Faivre, L., Locatelli, M.C., Mayençon, M., Sarcey, A., Broussolle, E., et al. (2010). A major determinant for binding and aminoacylation of tRNA(Ala) in cytoplasmic Alanyl-tRNA synthetase is mutated in dominant axonal Charcot-Marie-Tooth disease. Am. J. Hum. Genet. *86*, 77–82.
26. McLaughlin, H.M., Sakaguchi, R., Liu, C., Igarashi, T., Pehlivan, D., Chu, K., Iyer, R., Cruz, P., Cherukuri, P.F., Hansen, N.F., et al. (2010). Compound heterozygosity for loss-of-function lysyl-tRNA synthetase mutations in a patient with peripheral neuropathy. Am. J. Hum. Genet. *87*, 560–566.
27. Antonellis, A., Ellsworth, R.E., Sambuughin, N., Puls, I., Abel, A., Lee-Lin, S.Q., Jordanova, A., Kremensky, I., Christodoulou, K., Middleton, L.T., et al. (2003). Glycyl tRNA synthetase mutations in Charcot-Marie-Tooth disease type 2D and distal spinal muscular atrophy type V. Am. J. Hum. Genet. *72*, 1293–1299.
28. Jordanova, A., Irobi, J., Thomas, F.P., Van Dijck, P., Meerschaert, K., Dewil, M., Dierick, I., Jacobs, A., De Vriendt, E., Guergueltcheva, V., et al. (2006). Disrupted function and axonal distribution of mutant tyrosyl-tRNA synthetase in dominant intermediate Charcot-Marie-Tooth neuropathy. Nat. Genet. *38*, 197–202.

JOURNAL OF MAGNETIC RESONANCE IMAGING 35:418–425 (2012)

Original Research

Increased *N*-acetylaspartate in Model Mouse of Pelizaeus-Merzbacher Disease

Jun-ichi Takanashi, MD,[1,2*] Shigeyoshi Saito, PhD,[1] Ichio Aoki, PhD,[1] A. James Barkovich, MD,[3] Yukiko Ito, PhD,[4] and Ken Inoue, MD[4]

Purpose: To evaluate the *N*-acetylaspartate (NAA) and *N*-acetylaspartylglutamate (NAAG) biochemical pathways in the brain of *myelin synthesis-deficient* (*msd*) mouse, a model of Pelizaeus-Merzbacher disease (PMD).

Materials and Methods: We performed magnetic resonance imaging and proton magnetic resonance spectroscopy (^{1}H-MRS) of the thalamus for *msd* and wildtype mice with a 7.0 T magnet. NAA and NAAG were independently measured by high-performance liquid chromatography (HPLC). Immunohistochemical analysis using anti-Mbp, Gfap, Ng2, and NeuN antibodies were also performed.

Results: ^{1}H-MRS in *msd* mice revealed increased total NAA (tNAA, NAA+NAAG), creatine, glutamine, and glutamate and decreased choline (Cho). HPLC analysis revealed increases of both NAA and NAAG in the *msd* brains. Histologically, the *msd* brains revealed hypomyelination and astrogliosis. Oligodendrocyte progenitor cells and neurons were normal in number in the thalamus wherein ^{1}H-MRS was obtained.

Conclusion: The evidence suggests that the neurochemical derangement in the *msd* mice may be a primary increase of NAA resulting in a secondary increase of NAAG. Increased tNAA with decreased Cho detectable on ^{1}H-MRS may be an important marker for PMD, and might be used to distinguish it from more common neurological disorders that have decreased tNAA.

Key Words: magnetic resonance spectroscopy; *N*-acetylaspartate; *N*-acetylaspartylglutamate; hypomyelination; *myelin synthesis-deficient* mouse; Pelizaeus-Merzbacher disease

J. Magn. Reson. Imaging 2012;35:418–425.

PROTEOLIPID PROTEIN 1 (PLP1) is a major myelin protein of the mammalian central nervous system (CNS) with proposed functions in myelin membrane stability and maintenance. Mutations in the human *PLP1* gene lead to a broad clinical spectrum of hypomyelinating disorders ranging from the connatal (severe) and classic (mild) forms of Pelizaeus-Merzbacher disease (PMD) to spastic paraplegia type 2 (1,2). Reflecting hypomyelination, magnetic resonance imaging (MRI) of the brain in patients with PMD shows diffuse T_1 and T_2 prolongation to variable degrees, resembling the appearance in newborns (3).

Despite the progress in understanding the molecular basis and neuroimaging characteristics of PMD, the neurochemical basis associated with hypomyelination remains unknown. Proton magnetic resonance spectroscopy (^{1}H-MRS) allows a noninvasive exploration of tissue metabolism in vivo. The *N*-acetylaspartate (NAA) peak is useful for analysis of the brain by ^{1}H-MRS because N-acetyl protons are plentiful in the brain, and have a long T_2 relaxation time. As NAA is synthesized in neuronal mitochondria and is transported to axons, NAA is detected on ^{1}H-MRS both in the gray and white matter (with almost the same concentration). NAA is generally considered an important marker of viable, functioning neurons and axons (4,5). Many neurodegenerative disorders, therefore, exhibit a decrease of total NAA (tNAA; NAA at 2.01 ppm and *N*-acetylaspartylglutamate [NAAG] at 2.04 ppm, which are difficult to distinguish on clinical ^{1}H-MRS with a 1.5 or 3.0 T magnet) in the gray and white matter, including demyelinating leukodystrophies and neuronal degenerative disorders (6,7). An increase of tNAA, however, has been reported in patients with classic PMD, caused by *PLP1* duplications (8,9), and a female patient with undiagnosed hypomyelination disorder with normal *PLP1* gene (10). Thus far, it is not clear whether changes in the level of NAA or NAAG, or both, result in the increased tNAA. To evaluate this we performed ^{1}H-MRS on brains of *myelin synthesis-deficient*

[1]Molecular Imaging Center, National Institute of Radiological Sciences, Chiba, Japan.
[2]Department of Pediatrics, Kameda Medical Center, Kamogawa, Japan.
[3]Department of Radiology and Biomedical Imaging, University of California San Francisco, California, USA.
[4]Department of Mental Retardation and Birth Defect Research, National Institute of Neuroscience, National Center of Neurology and Psychiatry, Kodaira, Japan.
Contract grant sponsor: Ministry of Health, Labor and Welfare of Japan, Health and Labour Sciences Research Grants, Research on Intractable Diseases; Contract grant numbers: H22-Nanchi-Ippan-132 and H23-Nanchi-Ippan-78, Contract grant number: Research Grant (21B-5) for Nervous and Mental Disorders.
*Address reprint requests to: J.T., Department of Pediatrics, Kameda Medical Center, 929 Higashi-cho, Kamogawa-shi, Chiba 296-8602, Japan. E-mail: jtaka@kameda.jp
Received March 18, 2011; Accepted August 19, 2011.
DOI 10.1002/jmri.22817
View this article online at wileyonlinelibrary.com.

(*msd*) mice, a model of connatal PMD (11), and one of the most severely affected murine mutants of the *plp* gene, with a 7.0 T magnet and separately measured NAA and NAAG of the brains of these animals by high-performance liquid chromatography (HPLC).

MATERIALS AND METHODS

Animals

The experimental animals included postnatal day 21 (P21) *msd* mice with a spontaneous mutation (A242V) in the *plp1* gene (maintained in B6C3 background) and wildtype littermate mice. *Msd* mice are a model of connatal PMD, and develop progressive tremors and dystonia, which cause premature death around 1 month of age. The animals had free access to food and water and were kept under standard laboratory conditions of 22–23°C room temperature, around 50% humidity, and a 12:12 hour light/dark cycle. The study protocols were approved by the Animal Welfare Committee of the National Institute of Radiological Sciences and that of the National Center of Neurology and Psychiatry.

MRI Measurements

MRI and ^{1}H-MRS were performed for *msd* mice (n = 9, weight = 6.7 ± 1.4 g) and wildtype mice (n = 10, weight = 11.3 ± 1.2 g). Immediately prior to and during the MRI scanning, all mice were anesthetized with 2% isoflurane (Mylan Japan, Japan). The rectal temperature was continuously monitored and maintained at 36.5 ± 0.5°C using a heating pad throughout all experiments. During MRI scanning the mice lay in the supine position on an MRI-compatible cradle and were held in place by a handmade ear bar and anesthetized through a facemask with 2% isoflurane. All MRI experiments were performed on a 7.0 T MRI scanner (Magnet: Kobelco and JASTEC Japan; Console: Bruker Biospin, Germany) with a volume coil for transmission (Bruker) and a 2-ch phased array coil for reception (Rapid Biomedical, Germany). Coronal, sagittal, and axial multislice T_1-weighted imaging (T_1WI: multislice spin echo [SE]; repetition time [TR] / echo time [TE] = 400/9.57 msec; slice thickness = 1.0 mm; matrix = 256 × 256; field of view = 25.6 × 25.6 mm; number of repetitions = 2) was performed. Coronal T_2-mapping was performed using a multislice SE sequence (slice thickness = 1 mm; field of view = 25.6 × 25.6 mm; matrix = 128 × 128; number of repetitions = 1; TR = 3000 msec) with TE ranging from 20 to 100 msec in steps of 10 msec. T_2 values were calculated in the cortex, white matter, caudate-putamen, and thalamus with image analysis software, MRVision (Winchester, MA). The two-tailed Student's t-test was used to compare the T_2 values of the *msd* and wildtype mice.

^{1}H-MRS

For single-voxel ^{1}H-MRS, a region of interest (ROI) was chosen predominantly in the thalamus with a volume of interest of 3.0 × 3.0 × 3.0 mm, as determined on T_1WI (Fig. 1a,b). First- and second-order localized shimming was performed using the fast automatic shimming technique by mapping along projections (FASTMAP), resulting in a water line-width (full-width half-maximum line-width of the water signal) of below 14 Hz. The water signal was suppressed by variable power radiofrequency pulses with optimized relaxation delays. Outer volume suppression combined with a point-resolved spectroscopy sequence was used for signal acquisition (number of repetitions = 256; TR = 2500 msec; TE = 20 msec; spectral bandwidth = 4 kHz; number of data points = 2048; scan time = 10 min 42 sec).

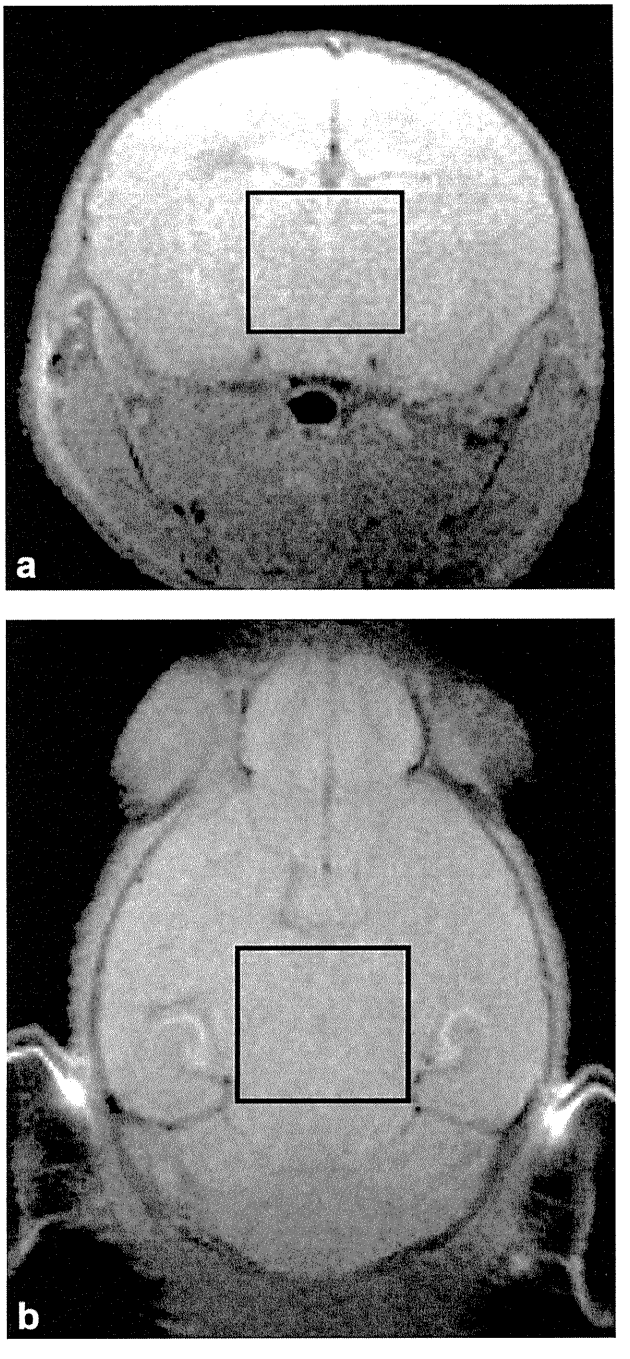

Figure 1. Coronal **(a)** and axial **(b)** T_1-weighted images show the thalamic ROI used for ^{1}H-MRS, with volume of 27 mm^3.

^{1}H-MRS was quantitatively analyzed using the water scaling method of LCModel, which uses the unsuppressed water signal obtained from the same ROI as an internal reference for quantification (default water proton density [PD] of 35.9M and exp(TE/T_2) = 0.7) (12,13). The concentration was corrected by the T_2 value of the ROI, as multiplied by R = exp (-20/T_2_ROI)/0.7); however, we used the default PD because we did not measure PD of the ROI. The concentrations of the metabolites were considered as having acceptable reliability when the LCModel showed percent of standard deviation (%SD, sometimes referred to as the Cramér-Rao lower bounds and expressed in percent of the estimated concentrations) less than 20; smaller %SD is associated with more reliable data (13,14). The mean concentration of each *msd* and wildtype mouse metabolite was compared using the two-tailed Student's *t*-test. Significance was set at $P < 0.0056$ (=0.05/9, 9 being the number of analyzed metabolite) after Bonferroni correction.

Measurement of NAA and NAAG by HPLC

Msd ($n = 8$) and wildtype ($n = 7$) mice at P21 were anesthetized with diethylether and perfused through the heart with ice-cold phosphate-buffered saline (PBS). These were different mice than those for the MRI and ^{1}H-MRS experiments, but were genetically the same. The brains were immediately removed and sliced into 1-mm-thick coronal sections, dissecting the thalamus and midbrain from four contiguous sections equivalent to bregma −0.94 to −4.96 mm on ice. These correspond to the areas examined by the MRI studies. Tissue samples were immediately frozen and stored at −80°C until required. The tissue preparation and the measurement of NAA and NAAG by HPLC were performed as described (15). In short, we applied the harvested samples (equivalent to 15 mg tissue) to pretreated SAX anion exchange columns (Bond Elut-SAX, Varian, Palo Alto, CA) followed by elution with 1 mL 5.88 mL/L phosphate acid (85%). The samples were injected onto a reversed-phase octadecyl column (C18) (4.6 μm × 250 mm; MCM, Japan) at 30°C. Standards for NAA and NAAG, prepared in the range of 0–100 μM, were used to determine their retention times for the peaks and to generate their linear standard curves. We measured NAA and NAAG simultaneously using the CoulArray System (ESA, Chelmsford, MA) with UV detector (ELITE LaChrom L-2400, Hitachi, Japan). We used the two-tailed Student's *t*-test for statistical analysis.

Immunohistochemical Analysis

Msd ($n = 3$) and wildtype ($n = 3$) mice at P21, that were different from those for MRI, ^{1}H-MRS, and HPLC analysis, were subjected to immunohistochemical analysis. They had the same genetic background and the immunochemical analysis was expected to represent those with MRI, ^{1}H-MRS, and HPLC analysis. We perfused the mice transcardially with 4% paraformaldehyde (PFA) in PBS and dissected and postfixed the brains overnight at 4°C. The brain samples were cryoprotected in 30% sucrose and mounted in OTC compound (Tissue-Tek, Sakura Fine Tek, Torrance, CA) and frozen. Coronal sections at 10 μm thickness were prepared for immunostaining. The following primary antibodies were used: mouse anti-Mbp antibody (1:1000; Covance, Denver, PA), mouse anti-Gfap antibody (1:500; Chemicon, Temecula, CA), rabbit anti-Ng2 antibody (1:200; Chemicon), and mouse anti-NeuN antibody (1:1000; Millipore, Bedford, MA; MAB377). For visualization, we utilized biotin-conjugated goat secondary antibody against each of host animal primary antibodies (1:200; Molecular Probes, Eugene, OR), avidin-biotin-horseradish peroxidase complex (Vectostain Elite ABC kit, Vector Laboratories, Burlingame, CA) and diaminobenzine (DAB detection kit, Vector). NG2- and NeuN-positive cells were counted at the dorsal parts of thalamus equivalent to bregma −1.22 to −2.46 mm.

RESULTS

MRI Findings and T_2 Value Measurement

Coronal T_2WI (TE = 80 msec of T_2 mapping) of *msd* mice typically demonstrated a three layered structure, ie, a high signal layer of white matter between the cortex and caudate putamen (Fig. 2a), which was difficult to distinguish in wildtype mice (Fig. 2b). The T_2 values of the cerebral cortex, white matter, caudate-putamen, and thalamus of *msd* and wildtype mice are shown in Table 1. The T_2 values of *msd* mice were significantly longer than those of wildtype mice in all examined regions. In *msd* mice the T_2 values of the white matter, caudate-putamen, and thalamus were longer than that of the cortex.

Brain Metabolites Measured by ^{1}H-MRS

The concentrations and %SD of each metabolite in *msd* and wildtype mice are shown in Table 2. The %SD of tNAA (NAA+NAAG), creatine (Cr), choline (Cho), myo-Inositol (mIns), glutamate (Glu), and taurine (Tau) in all *msd* and wildtype mice were less than 10, and the mean %SD of these metabolites were less than 6. The %SD of other metabolites, such as glutamine (Gln), guanine (Gua), and gamma-aminobutyric acid (GABA), were less than 20 in all *msd* and wildtype mice. In the *msd* mice, tNAA, Cr, Glu, and Gln were elevated and Cho was decreased (Fig. 3a), compared with wildtype mice (Fig. 3b). There were no differences in mIns, Tau, Gua, and GABA between the two groups.

Although NAAG in the *msd* mice (0.68 ± 0.29 mM) was elevated compared with those in wildtype mice (0.23 ± 0.23 mM), these results were not considered reliable because only two of the *msd* mice and none of the wildtype mice showed NAAG concentrations with %SD of less than 20 (%SD being 37.9 ± 29.6 in *msd* mice, 414 ± 467 in wildtype mice).

Measurement of NAA and NAAG by HPLC

The NAA and NAAG levels in *msd* and wildtype mice in the thalamus are shown in Table 3. Both NAA and

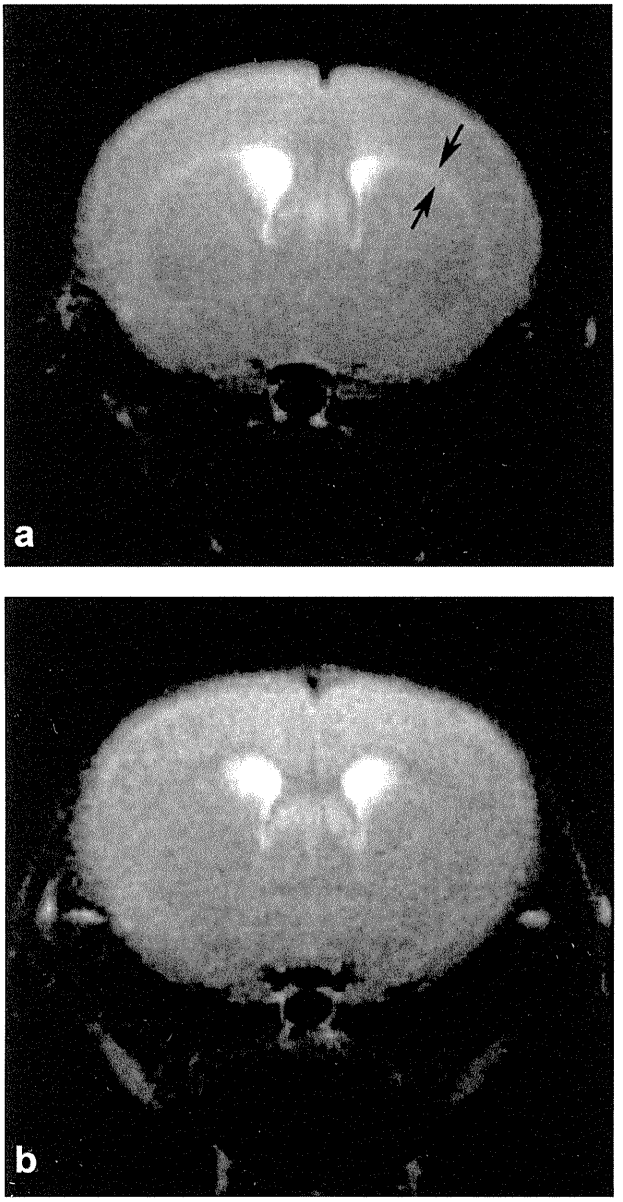

Figure 2. T_2-weighted image of a *msd* mouse **(a)** shows a high intensity band of unmyelinated white matter (arrows) between the cortex and caudate putamen. T_2-weighted image of the wildtype mouse **(b)** shows a slightly low signal intensity band of myelinated white matter in the same location.

NAAG levels in *msd* mice were higher than those in wildtype mice.

Immunohistochemical Analysis

Immunostaining of Mbp, a marker for mature myelin sheath in *msd* mice, showed sparse and weak staining in the white matter, thalamus, and cortex in comparison with the wildtype (Fig. 4a,b). Gfap immunostaining, a marker for astrocytes, of the *msd* brain showed dense and strong staining and an increase of positive cells compared with the wildtype (Fig. 4c,d). These indicated hypomyelination and astrogliosis in the *msd* brain at P21. Ng2 immunostaining, a marker for oligodendrocyte progenitor cells (OPC), of the *msd* brain revealed increased immunoreactivity in the white matter, but no obvious difference in the thalamus, compared with the wildtype (Fig. 4e-J). The number of the Ng2 positive cells in the thalamus was almost same in both mice (123 ± 17 cells/mm^2 in *Msd* brain vs. 125 ± 7 cells/mm^2 in the wildtype brain). The number of the NeuN immunostaining (a marker for neuronal cells) positive cells in the thalamus was almost equal in both mice (874 ± 109 cells/mm^2 in *Msd* brain vs. 876 ± 53 cells/mm^2 in the wildtype brain).

DISCUSSION

The most important findings in this study were that the tNAA was increased in *msd* mice (a model of connatal PMD) on ^{1}H-MRS and that this increase of tNAA resulted from increase of both NAA and NAAG. The number of neurons in the thalamus (ROI of ^{1}H-MRS) was almost the same in both *msd* and wildtype mice, which suggests that increased NAA (rich in neuron) in *msd* mice brain do not result from the increased neurons per se, but reflect some other factors. An increase of both NAA and NAAG are compatible with the reports of increased tNAA in patients with PMD (8,9), and with those of increased NAAG in the cerebrospinal fluid (CSF) in patients with hypomyelinating disorders, including PMD (16), Pelizaeus-Merzbacher-like disease (17), free sialic acid storage disease (18), and an undiagnosed hypomyelinating disorder (10).

Why does the *msd* brain have an increase of both NAA and NAAG? NAA is one of the most highly abundant free amino acids in the CNS (around 10 mM in man). It is synthesized in neuronal mitochondria from acetyl CoA and aspartate, catalyzed by *L*-aspartate *N*-acetyltransferase (Asp-NAT). NAA is either released from the neuron or transported to oligodendrocytes, where it is catabolized by aspartoacylase (ASPA) into acetate and aspartate; these are used for fatty acid and steroid synthesis and for energy production. NAA is also the precursor for the synthesis of NAAG in neurons (5,6). The biosynthesis or regulatory mechanisms of NAAG is poorly understood; however, it modulates glutamatergic synaptic transmission; it is released from neuronal synapses along with other neurotransmitters. Extracellular NAAG is hydrolyzed

Table 1
T2 Value of Each Region of *msd* and Wildtype Mice

	Cortex (msec)	WM (msec)	CPu (msec)	Th (msec)
Msd (n = 9)	51.4 ± 0.9	55.4 ± 1.0	54.7 ± 1.1	55.9 ± 0.9
Wild (n = 10)	49.7 ± 1.1	49.5 ± 1.1	51.4 ± 1.2	52.5 ± 0.9
P-value	<0.01	<0.001	<0.001	<0.001

WM, white matter; CPu, caudate-putamen; Th, thalamus.

Table 2
Concentration of Metabolites on ^{1}H-MRS

		tNAA	Cr	Cho	mIns
Msd	Concentration (mM)	7.10 ± 0.31	6.16 ± 0.31	1.11 ± 0.06	4.13 ± 0.42
$n = 9$	%SD	3.5 ± 0.7	2.3 ± 0.5	3.6 ± 0.5	5.9 ± 0.9
Wild	Concentration (mM)	5.32 ± 0.50	5.61 ± 0.15	1.42 ± 0.10	4.19 ± 0.50
$n = 10$	%SD	3.6 ± 0.9	2.4 ± 0.7	3.0 ± 0	5.5 ± 0.9
p value		<0.001	<0.001	<0.001	NS
	Gln	Glu	Tau	Gua	GABA
	4.23 ± 0.47	7.43 ± 0.41	7.25 ± 0.88	1.55 ± 0.51	2.67 ± 0.62
	8.2 ± 1.0	4.0 ± 0.5	3.5 ± 0.7	12.9 ± 3.0	13.5±3.0
	3.81 ± 0.54	6.31±0.31	6.30±0.48	1.42±0.37	2.44 ± 0.31
	10.8 ± 2.3	5.5 ± 0.8	5.5 ± 0.8	14.2 ± 3.2	13.4 ± 1.9
	<0.005	<0.001	NS	NS	NS

tNAA, N-acetylaspartate and N-acetylaspartylglutamate; Cr, creatine; Cho, choline; mIns, myo-Inositol; Gln, glutamine; Glu, glutamate; Tau, taurine; Gua, guanine; GABA, γ-aminobutyric acid.
P-value was analyzed in each metabolite between *msd* and wild mouse.

into NAA and Glu by glutamate carboxypeptidase II (GCPII) on the membrane surface of astrocytes; the breakdown products are then taken in by the astrocytes (5). Accordingly, NAA and NAAG have been purported to have axon-oligodendrocyte and axon-astrocyte signaling functions, respectively.

In *msd*, mutant plp1 proteins are abnormally folded and they accumulate in the endoplasmic reticulum, resulting in the activation of an unfolded protein response that finally leads to oligodendrocyte apoptotic cell death before normal myelination occurs (19). The absence or dysfunction of mature myelinating oligodendrocytes, where NAA is catabolized by ASPA (20), may either disable the neuron-to-oligodendrocyte NAA transport or affect NAA catabolism in oligodendrocytes. Either way, NAA would be accumulated in neurons, probably resulting in increased tNAA on ^{1}H-MRS. Because elevated NAA concentration increases NAAG biosynthesis (5), NAAG may be secondarily increased. In agreement with this hypothesis, CFS of patients with Canavan disease, which is caused by mutations in the *ASPA* gene, showed increased NAA and NAAG (16).

Two alternative mechanisms can be considered based on previous studies. First, some studies showing increased NAAG in the CSF of patients with various hypomyelinating disorders suggested an impaired function of GCPII on astrocyte membranes, which normally hydrolyzes NAAG into NAA and Glu (10,16,18). This mechanism, however, would not explain the increase of NAA observed in our study, because GCPII inhibition actually increases the level of NAAG and decreases the level of Glu (21), and presumably decrease its enzymatic by-product, NAA.

Second, a potentially increased number of OPC may enhance NAA and NAAG levels. In *Msd* and also in another PMD mouse model, *jimpy*, massive apoptosis of differentiating oligodendrocytes appears to induce the proliferation of OPC in the white matter (22,23). Primary cultures of rat OPC exhibited the NAA concentration higher than neurons (24,25). If the number of OPC is increased within the *msd* brains, NAA and NAAG can be increased. Ng2 immunostaining on *msd* mice at P21, however, revealed no change in number of OPC in the thalamus (Fig. 4), where ^{1}H-MRS was mainly obtained. Therefore, the number of OPC in ROI seems unlikely to be the major factor underlying increased tNAA in *msd* mice, at least in our study, although we cannot exclude the possibility that ^{1}H-MRS may contain signals from white matter, where strong Ng2 immunoreactivity was observed in *msd*, as a partial volume effect.

Altogether, we hypothesized the most probable mechanism for the increase of both NAA and NAAG in *msd* mice is that an absence or dysfunction of oligodendrocytes may result in a primary increase of NAA, which would then lead to secondary increase of NAAG. Currently, the cellular mechanisms to cause disruption of either catabolism or neuroglial transport of NAA remain undetermined. Elucidation of this pathological process is required for the validation of our hypothesis.

Other detectable metabolites in the *msd* mice also showed changes similar to those often observed in patients with PMD: a reduction of Cho and an elevation of Cr (8,9). The Cho peaks likely contain various cell membrane precursor or breakdown products such as phosphocholine, glycerophosphocholine, and phosphatidylcholine. The reduction of Cho may be explained by the severe retardation of myelination and the diminished number of oligodendrocytes in *msd* mice brain (Fig. 4a,b) (22,23,26).

The Cr peak is composed of both phosphocreatine and free Cr, which are present in both neuronal and glial cells. In rats, astrocytes and oligodendrocytes have Cr concentrations twice and four times as high, respectively, as those observed in neurons (24). As reactive astrogliosis with decreased oligodendrocytes is observed in *msd* mice brain (Fig. 4c,d), the elevated Cr observed on ^{1}H-MRS may result from the increased number of astrocytes, which compensates for decreased number of oligodendrocytes.

Finally, some discussion is necessary for the ^{1}H-MRS in this study. Regarding the ROI placement, we were unable to locate the ROI in the white matter because the white matter of mice is too thin to allow placement of a 3 × 3 × 3 mm voxel. Because the normal thalamus is composed of a mixture of myelinated axons and cellular components, eg, neurons, ^{1}H-MRS in *msd* mice may reflect metabolic derangements of

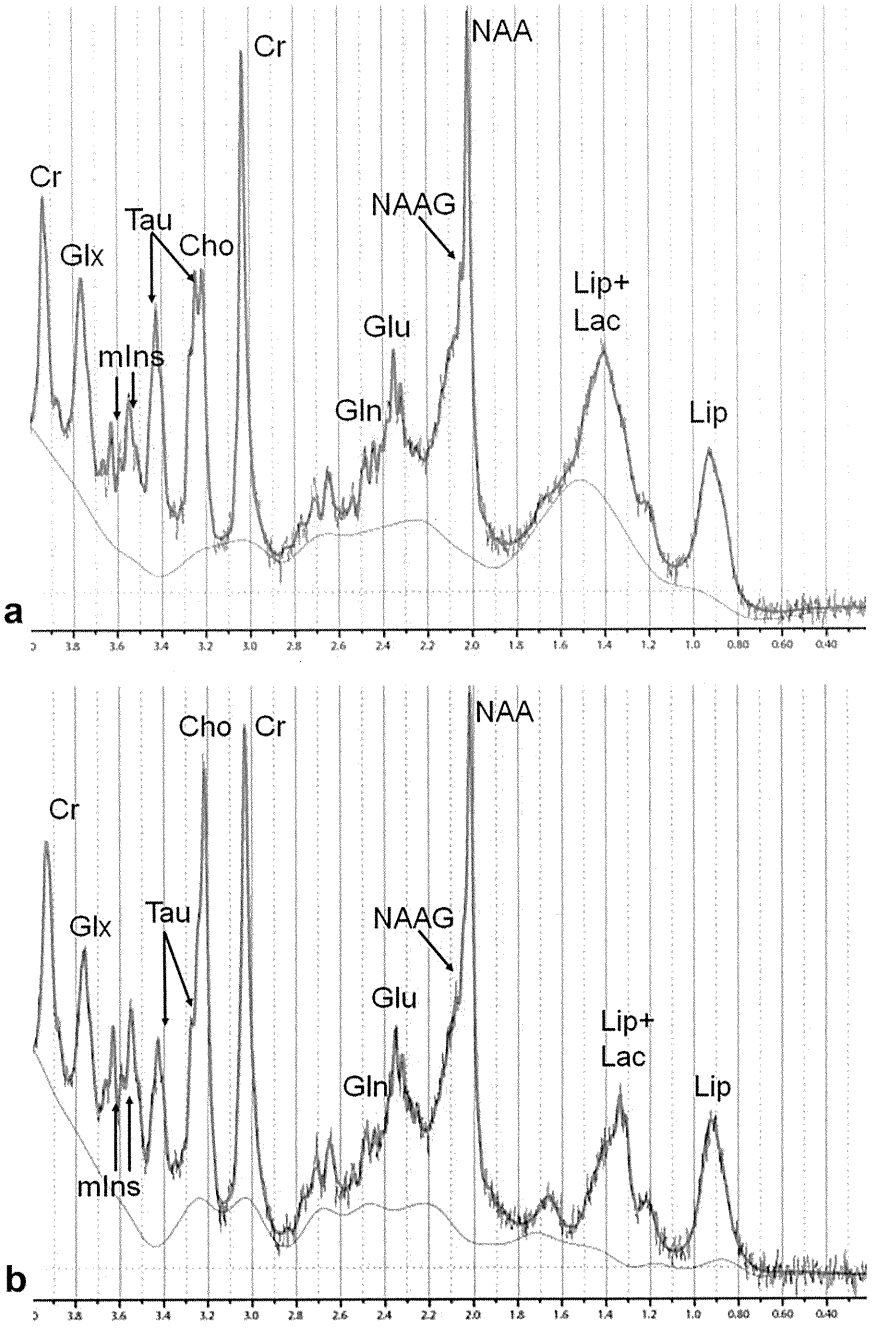

Figure 3. ^{1}H-MRS of a *msd* mouse **(a)** shows markedly reduced Cho compared with in a wildtype mouse **(b)**. [Color figure can be viewed in the online issue, which is available at wileyonlinelibrary.com.]

both components. Mbp immunostaining indicated hypomyelination in the *msd* brain, not only in the white matter, but also in the thalamus (Fig. 4a–d), as observed in patients with PMD (26). Reflecting the pathology, *msd* mice exhibited longer T_2 values than wildtype mice in the all regions examined by MRI, including the thalamus (Table 1). These suggest that ^{1}H-MRS in the thalamus reasonably reflect metabolic derangements associated with hypomyelination. On the other hand, the number of neurons in the thalamus was almost same in both *msd* and wildtype mice. The thalamus, therefore, was expected to show similar metabolic derangement associated with hypomyelination to that found in the white matter.

The concentrations of metabolites were corrected by the LCModel by entering the T_2 value of the ROI, but could not correct by the proton density (PD).

Table 3
NAA and NAAG Analyzed by HPLC

	NAA	NAAG	
Msd ($n = 8$)	3.52 ± 0.37	0.66 ± 0.06	μmol/g tissue
Wild ($n = 7$)	2.90 ± 0.43	0.57 ± 0.07	μmol/g tissue
P-value	<0.01	<0.05	

NAA, *N*-acetylaspartate; NAAG, *N*-acetylaspartylglutamate.

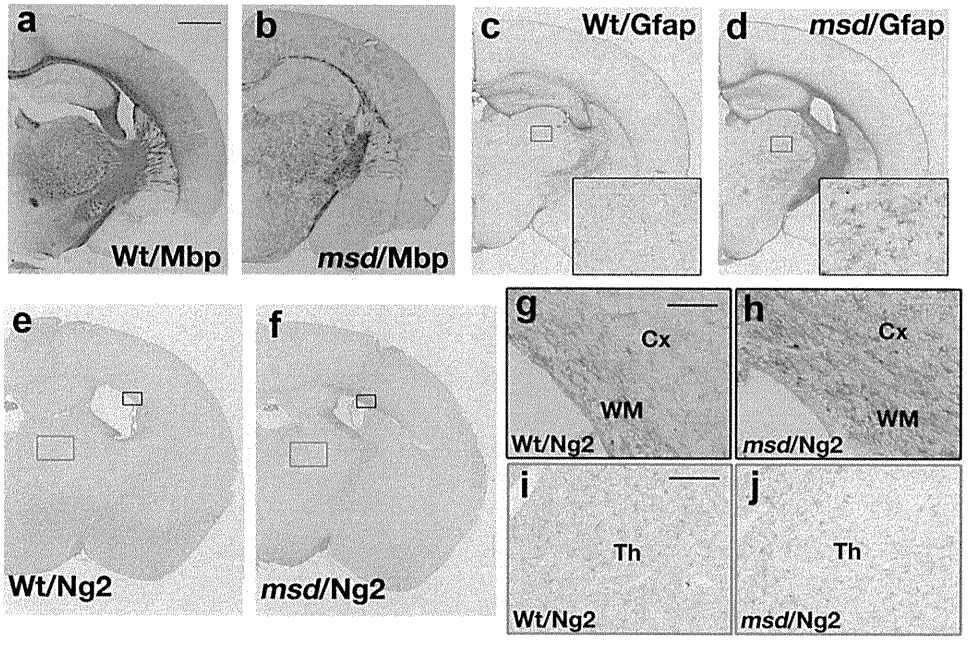

Figure 4. Immunostaining of coronal sections from wildtype (WT; a,c,e,g,I) and *msd* (b, d, f, h, j) mouse brains. **a,b:** Mbp immunostaining. *Msd* brain (b) shows sparse and weak staining in the white matter, cortex, and the thalamus in comparison with in the wildtype (a), indicating diminished myelination. **c,d:** Gfap immunostaining. Area in the boxes in c,d are magnified to insets in c,d. *Msd* brain (d) shows dense and strong staining in the white matter and thalamus, compared with in the wildtype (c), indicating reactive astrogliosis. **e–j:** Ng2 immunostaining. g–j: High magnification of black box (white matter [WM] and cortex [Cx]) and red box (thalamus [Th]) in e,f, respectively. Note that *Msd* shows increased immunoreactivity in the white matter (h), but not in the thalamus (j), compared with WT mouse (g,i). Scale bars = 1 mm in a–f; 100 μm in g,h; 200 μm in i,j.

Because the PD is expected to be higher in *msd* mice than in wildtype mice, an additional correction with PD (multiplied by R = PD_ROI/35.9) (13) would make the concentrations in *msd* mice larger relative to those in wildtype mice. We were able to approximate the ratio of PDs in *msd* and wildtype mice from the signal intensity on T_2-mapping (minimum TE of 20 msec) and the T_2 value of the thalamus, which suggested that PD of *msd* mice in the thalamus might be 5.8% higher than wildtype mice. Therefore, we suggest that the additional PD correction, if it had been possible, may not have affected the results of this ^{1}H-MRS study. We could not reliably measure NAAG with ^{1}H-MRS and, therefore, performed additional analysis with HPLC. Further studies at a higher magnetic field, such as 11 T, or using more sensitive coils should enable us to measure NAAG using only ^{1}H-MRS.

In conclusion, this study revealed an increase of both NAA and NAAG in *msd* mice, a model of connatal PMD, possibly resulting from a primary increase of NAA with resultant secondary increase of NAAG. Increased tNAA with decreased Cho may be an important marker for PMD, allowing distinction from most common neurological disorders in which tNAA is generally decreased.

ACKNOWLEDGMENTS

We thank Ms. Sayaka Shibata (Molecular Imaging Center, National Institute of Radiological Sciences, Chiba) and Ms. Eriko Arima (National Institute of Neuroscience, National Center of Neurology and Psychiatry, Tokyo) for technical support.

REFERENCES

1. Inoue K. PLP1-related inherited dysmyelinating disorders: Pelizaeus-Merzbacher disease and spastic paraplegia type 2. Neurogenetics 2005;6:1–16.
2. Lee JA, Inoue K, Cheung SW, Shaw CA, Stankiewicz P, Lupski JR. Role of genomic architecture in PLP1 duplication causing Pelizaeus-Merzbacher disease. Hum Mol Genet 2006;15: 2250–2265.
3. Takanashi J, Sugita K, Tanabe Y, et al. MR-revealed myelination in the cerebral corticospinal tract as a marker for Pelizaeus-Merzbacher disease with proteolipid protein gene duplication. AJNR Am J Neuroradiol 1999;20:1822–1828.
4. Moffett JR, Namboodiri MAA. Expression of N-acetylaspartate and N-acetylaspartylglutamate in nervous system. Adv Exp Med Biol 2006;576:7–26.
5. Moffett JR, Ross B, Arun P, Madhavarao CN, Namboodiri AM. N-acetylaspartate in the CNS: from neurodiagnostics to neurobiology. Prog Neurobiol 2007;81:89–131.
6. Cecil KM, Kos RS. Magnetic resonance spectroscopy and metabolic imaging in white matter diseases and pediatric disorders. Top Magn Reson Imaging 2006;17:275–293.
7. Van der Voorn JP, Pouwels PJ, Hart AA, et al. Childhood white matter disorders: quantitative MR imaging and spectroscopy. Radiology 2006;241:510–517.
8. Takanashi J, Inoue K, Tomita M, et al. Brain N-acetylaspartate is elevated in Pelizaeus-Merzbacher disease with PLP1 duplication. Neurology 2002;58:237–241.
9. Hanefeld FA, Brockmann K, Pouwels PJW, Wilken B, Frahm J, Dechent P. Quantitative proton MRS of Pelizaeus-Merzbacher disease: evidence of dys- and hypomyelination. Neurology 2005;65: 701–706.
10. Wolf NI, Willemsen MA, Engelke UF, et al. Severe hypomyelination associated with increased levels of N-acetylaspartylglutamate in CSF. Neurology 2004;62:1503–1508.

11. Komaki H, Sasaki M, Yamamoto T, Iai M, Takashima S. Connatal Pelizaeus-Merzbacher disease associated with the jimpy (msd) mice mutation. Pediatir Neurol 1999;20:309–311.
12. Provencher SW. Automatic quantitation of localized in vivo ^{1}H spectra with LCModel. NMR Biomed 2001;14:260–264.
13. Provencher SW. LCModel & LCMgui user's manual. LCModel Version 6.2-3 http://s-provencher.com/pub/LCModel/manual/manual.pdf
14. Atwood T, Robbins ME, Zhu J-M. Quantitative in vivo proton MR spectroscopic evaluation of the irradiated rat brain. J Magn Reson Imaging 2007;26:1590–1595.
15. Reynolds LM, Cochran SM, Morris BJ, Pratt JA, Reynolds GP. Chronic phencyclidine administration induced schizophrenia-like changes on N-acetylaspartate and N-acetylaspartylglutamate in rat brain. Schizophr Res 2005;73:147–152.
16. Burlina AP, Ferrari V, Burlina AB, et al. N-acetylaspartylglutamate (NAAG) in Pelizaeus-Merzbacher disease. Adv Exp Med Biol 2006;576:353–359.
17. Sartori S, Burlina AB, Salviati L, et al. Increased level of N-acetylaspartylglutamate (NAAG) in the CSF of a patient with Pelizaeus-Merzbacher-like disease due to mutation in the GJA12 gene. Eur J Paediatr Neurol 2008;12:348–350.
18. Mochel F, Engelke UF, Barritault J, et al. Elevated CSF N-acetylaspartylglutamate in patients with free sialic acid storage diseases. Neurology 2010;74:302–305.
19. Gow A, Southwood CM, Lazzarini RA. Disrupted proteolipid protein trafficking results in oligodendrocyte apoptosis in an animal model of Pelizaeus-Merzbacher disease. J Cell Biol 1998;140: 925–934.
20. Bhakoo KK, Craig TJ, Styles P. Developmental and regional distribution of aspartoacylase in rat brain tissue. J Neurochem 2001;79:211–220.
21. Ghadge GD, Slusher BS, Bodner A, et al. Glutamate carboxypeptidase II inhibition protects motor neurons from death in familial amyotrophic lateral sclerosis models. Proc Natl Acad Sci U S A 2003;100:9554–9559.
22. Nishiyama A. Glial progenitor cells in normal and pathological states. Keio J Med 1998;47:205–208.
23. Skoff RP. Increased proliferation of oligodendrocytes in the hypomyelinating mouse mutant-jimpy. Brain Res 1982;248: 19–31.
24. Urenjak J, Williams SR, Gadian DG, Noble M. Proton nuclear magnetic resonance spectroscopy unambiguously identifies different neural cell types. J Neurosci 1993;13:981–989.
25. Bhakoo KK, Pearce D. In vitro expression of *N*-acetyl aspartate by oligodendrocytes: implication for proton magnetic resonance spectroscopy signal in vivo. J Neurochem 2000;74:254–262.
26. Seitelberger F. Neuropathology and genetics of Pelizaeus-Merzbacher disease. Brain Pathol 1995;5:267–273.

RESEARCH ARTICLE

AMERICAN JOURNAL OF medical genetics PART A

A New Microdeletion Syndrome of 5q31.3 Characterized by Severe Developmental Delays, Distinctive Facial Features, and Delayed Myelination

Keiko Shimojima,[1] Bertrand Isidor,[2] Cédric Le Caignec,[2,3] Akiko Kondo,[4] Shinji Sakata,[4] Kousaku Ohno,[4] and Toshiyuki Yamamoto[1]*

[1]Tokyo Women's Medical University Institute for Integrated Medical Sciences, Tokyo, Japan

[2]Service de Génétique Médicale, Centre Hospitalier Universitaire de Nantes 7, Nantes, France

[3]INSERM, UMR915, l'institut du Thorax, Nantes, France

[4]Division of Child Neurology, Institute of Neurological Sciences, Faculty of Medicine, Tottori University, Yonago, Japan

Received 21 July 2010; Accepted 10 December 2010

Chromosomal deletion including 5q31 is rare and only a few patients have been reported to date. We report here on the first two patients with a submicroscopic deletion of 5q31.3 identified by microarray-based comparative genomic hybridization. The common clinical features of both patients were marked hypotonia, feeding difficulty in infancy, severe developmental delay, and epileptic/nonepileptic encephalopathy associated with delayed myelination. Both patients also shared characteristic facial features, including narrow forehead, low-set and abnormal auricles, bilateral ptosis, anteverted nares, long philtrum, tented upper vermilion, edematous cheeks, and high palate. The deleted region contains clustered PCDHs, including and *PCDHG*, which are highly expressed in the brain where they function to guide neurons during brain development, neuronal differentiation, and synaptogenesis. The common deletion also contains neuregulin 2 (*NRG2*), a major gene for neurodevelopment. We suggest that 5q31.3 deletion is responsible for severe brain developmental delay and distinctive facial features, and that the common findings in these two patients representing a new microdeletion syndrome. We need further investigations to determine which genes are responsible for the patients' characteristic features. © 2011 Wiley-Liss, Inc.

Key words: microdeletion; 5q31.3; array-based comparative genomic hybridization (aCGH); developmental delay; protocadherin (PCDH); neuregulin 2 (*NRG2*)

How to Cite this Article:
Shimojima K, Isidor B, Caignec CL, Kondo A, Sakata S, Ohno K, Yamamoto T. 2011.
A new microdeletion syndrome of 5q31.3 characterized by severe developmental delays, distinctive facial features, and delayed myelination.
Am J Med Genet Part A 155:732–736.

INTRODUCTION

Interstitial deletions of the long arm of chromosome 5 are rare, except in the 5q35.2q35.2 region that includes the 2-Mb *NSD1* locus which is associated with Sotos syndrome [Visser and Matsumoto, 2003]. Although patients with proximal deletions that encompass the 5q15 to q22 region experience mild developmental delays, those with distal deletions that encompass the 5q22 to q31 region are more severely handicapped, fail to thrive, and present with significant craniofacial dysmorphism and joint dislocations or contractures [Garcia-Minaur et al., 2005]. Furthermore, there are only a few reports of patients with deletions encompassing the 5q31.3 region [Felding and Kristoffersson, 1980; Kramer et al., 1999; Arens et al., 2004].

Recently, we encountered 2 patients with severe developmental delay and distinctive facial features. Microarray-based comparative genomic hybridization (aCGH) analyses identified a common microdeletion of 5q31 in both patients. Radiological examination yielded characteristic finding with delayed myelination in both patients. The details of these cases are discussed in this report. Data on the patients were deposited in the DECIPHER database (Database of Chromosomal Imbalances and Phenotype in Humans using Ensembl Resources, https://decipher.sanger.ac.uk), and the corresponding DECIPHER number is given.

Grant sponsor: Hayashi Memorial Foundation for Female Natural Scientists (to K. Shimojima).
*Correspondence to:
Toshiyuki Yamamoto, M.D., Ph.D., Tokyo Women's Medical University Institute for Integrated Medical Sciences, 8-1 Kawada-Cho, Shinjuku-Ward, Tokyo 162-8666, Japan. E-mail: toshiyuki.yamamoto@twmu.ac.jp
Published online 15 March 2011 in Wiley Online Library (wileyonlinelibrary.com).
DOI 10.1002/ajmg.a.33891

CLINICAL REPORTS

Patient 1 (DECIPHER #TWM253734)

A Japanese boy was born at 40 weeks 5 days gestation by caesarean when labor had failed to begin. He is the first child of a 30-year-old father and a 26-year-old mother at the time of his birth. His birth weight was 2,925 g (−0.3 SD), length 50 cm (+0.5 SD), and head circumference 35 cm (+1.3 SD). Postaxial polydactyly of the right hand was noted. Patent ductus arteriosus (PDA) and a small ventricular septal defect (VSD) were revealed by echocardiography; PDA was surgically treated when he was 52 days old, and the small VSD was observed but not treated. He showed failure to thrive due to severe hypotonia and feeding difficulty, and aspiration was suspected because of recurrent pneumonia. Tube feeding was initiated at 6 months of age. Although he had no epileptic episodes, his electroencephalography showed spike waves on the right side of the posterior and occipital regions during natural sleep. Auditory brainstem response revealed obscure III waves in both sides, and the threshold was 40 dB. His median nerve conductive velocity (NCV) showed a delay with 32.5 m/s (−2.1 SD) on the left and 30.5 m/s (−2.5 SD) on the right. His posterior tibial NCV was also revealed to be delayed with 27.6 m/s (−3.2 SD) on both sides. These findings indicated peripheral neuropathy.

At 18 months of age, he showed delayed growth and microcephaly with height 76.4 cm (−1.6 SD), weight 8.7 kg (−1.7 SD), and head circumference 42.8 cm (−3.0 SD). He showed distinctive features including narrow forehead, low-set and abnormal auricles, bilateral ptosis, epicanthic folds, depressed nasal bridge, anteverted nares, long philtrum, tented upper vermilion, edematous cheeks, and high palate (Fig. 1A). His developmental milestones were markedly delayed with no contact eye movements, no smile response, and no head control. Brain magnetic resonance imaging (MRI) revealed reduced volume of the cerebrum and severely delayed myelination (brain appearance was that of an 8-month-old child) in T2-weighted imaging (Fig. 2A). Chromosomal G-banding showed a normal male karyotype.

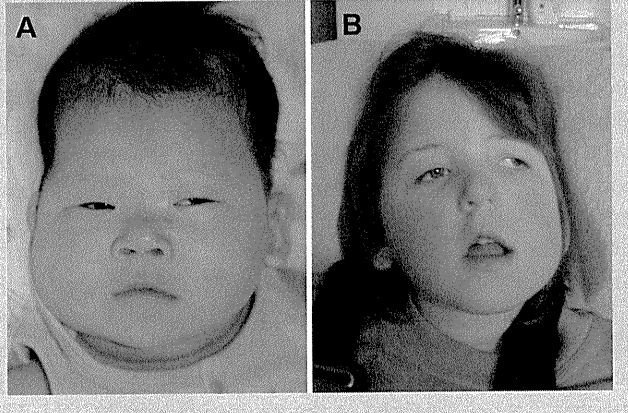

FIG. 1. Patient facial features. (A) Patient 1 at 18 months old. (B) Patient 2 at 6 years old.

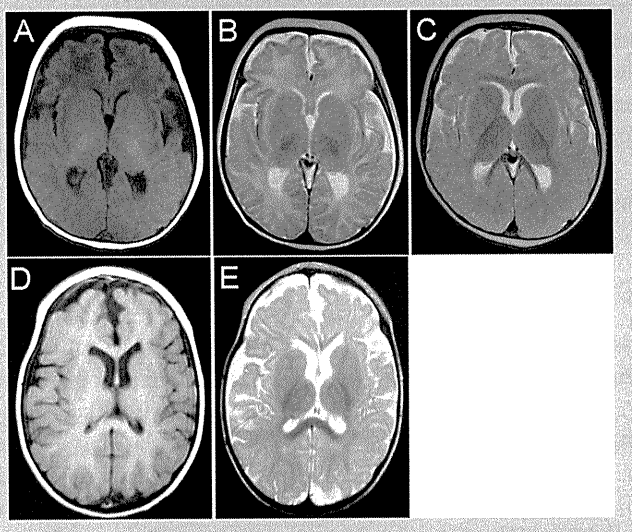

FIG. 2. Brain MRI findings with T1-weighted images (A, D) and T2-weighted images (B, C, E). Patient 1 at 4 months (A, B) and 18 months old (C). Patient 2 at her age of 4 years and 4 months old (D, E). Both patients showed reduced volume of the cerebrum associated with hypomyelination.

Patient 2 (DECIPHER #4681)

An 8-year-old French girl had no family history and no consanguinity in her parents. There was no complication during pregnancy. She was born with a birth weight of 3,700 g (+0.5 SD), a length of 52 cm (+1.0 SD), and a head circumference of 36 cm (+1.0 SD). Since early infancy, she showed feeding difficulties due to severe hypotonia. She had severe developmental delay with sitting at 11 months. Since the age of 12 months, she suffered epileptic seizures which were drug-resistant (hydrocortisone, clonazepam, topiramate, lamotrigine). Her epileptic status was diagnosed as Lennox–Gastaut syndrome.

She was of relatively small stature at a height of 121 cm (−1.5 SD), had a weight of 16.7 kg (−2.5 SD), and head circumference of 50 cm (−1.5 SD). She was not able to walk unassisted and was apraxic for speech. Her features were distinctive with narrow forehead, low-set ears, bilateral ptosis, downslanting palpebral fissures, anteverted nares, long philtrum, tented upper vermilion, edematous cheeks, and high palate (Fig. 1B). Strabismus was also noted. Brain MRI examination showed ventriculomegaly with reduced volume of the cerebrum, particularly in the frontoparietal regions, and marked hypomyelination (Fig. 2B). Conventional chromosome analysis showed a normal female karyotype.

MATERIALS AND METHODS

For further evaluation, microarray-based comparative genomic hybridization (aCGH) analyses, using Human Genome CGH Microarray 105A for Patient 1 and 44A for Patient 2 (Agilent Technologies, Santa Clara, CA), were performed according to the manufacturer's protocol, with genomic DNAs extracted from

peripheral blood samples. The identified aberrations were confirmed by fluorescence in situ hybridization (FISH) analyses, and both patients were also analyzed by FISH. Parental origin of the deletion in Patient 1 was determined using the microsatellite marker D5S1979 according to methods described elsewhere [Komoike et al., 2010]. Information regarding the primers used for the marker was obtained from the in-silico library (http://genome.ucsc.edu/).

RESULTS

Losses of genomic copies of 5q31.3 were identified in both patients. Patient 1 showed a 5.0-Mb deletion with molecular karyotyping as arr chr5q31.2q31.3(137,538,788–142,574,719)(hg18)x1 and Patient 2 showed a 2.6-Mb deletion with molecular karyotyping as arr chr5q31.3q31.3(139,117,448–141,682,547)(hg18)x1 (Fig. 3). FISH analyses with only one signal for the targeted probe confirmed the deletion (Fig. 4), and subsequent parental FISH analyses using the same probe showed no abnormality in their parents (data not shown), indicating de novo occurrence. Patient 1 shared the D5S1979 allele with his mother but not with his father (Fig. 4). This indicated that the deletion was paternally derived, and the final karyotype was ish del(5)(q31.2q31.3)(RP11-678N8x1) dn pat.

DISCUSSION

Both the patients in the present study showed an overlapping deletion of the region that included 5q31.3. The clinical features that were common for both patients were marked hypotonia, feeding difficulties in infancy, severe developmental delay, and epileptic/nonepileptic encephalopathy. Both patients also showed similar characteristic facial features, including a narrow forehead, low-set and abnormal auricles, bilateral ptosis, anteverted nares, long philtrum, tented vermilion of the upper lip, edematous cheeks, and high palate. Another characteristic finding was delayed myelination of the white matter, as identified by MRI examination. Thus, these findings are consistent, recognizable, and clinical features of 5q31.3 deletion.

To the best of our knowledge, five reports on patients with chromosome 5q31 deletions are available in the literature (Fig. 5). The first patient reported by Felding and Kristoffersson had manifestations similar to those of our patients [Felding and Kristoffersson, 1980]. Kramer et al. [1999] reported on a patient with 5q31q33 deletion whose condition was severely impaired; this patient showed congenital anomalies and died in the neonatal period. Arens et al. [2004] reported a patient with 5q22.1q31.3 deletion whose clinical findings included growth retardation, moderate psychomotor retardation, and mild facial dysmorphisms were similar to those of our patients. However, the severity of the developmental delay was milder than that of our patients, because she could walk without support and could speak a few words. These three patients were suspected to carry deletions of 5q31.3, but the deletion regions were ambiguous in conventional G-banding examination, and no neuroimaging test was available. We were thus unable to compare these patients with ours.

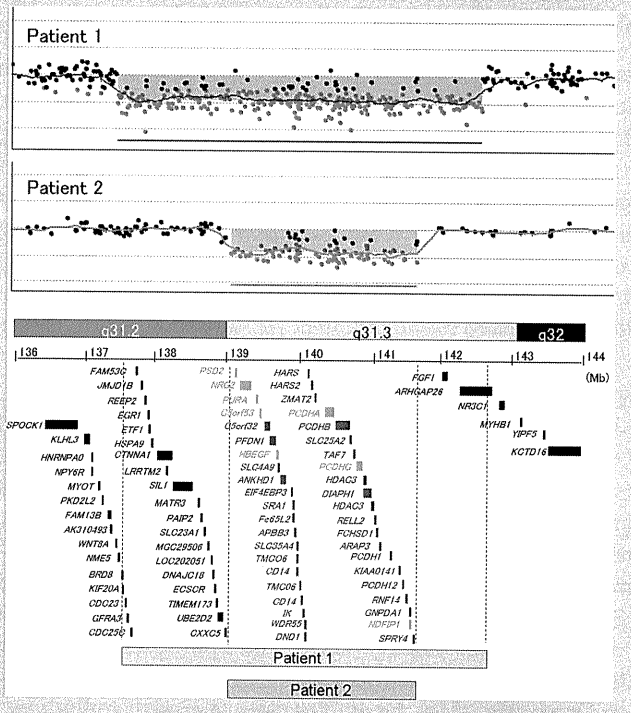

FIG. 3. The results of aCGH for chromosome 5. The aberrant areas of chromosome 5q31.2q31.3 are expanded in "Gene View" using CGH Analytics version 4.0 (Agilent) with the ADM-2 algorithm at a threshold of 6.0. The vertical axis indicates gain or loss of genome copy number and the horizontal axis indicates the physical position on chromosome 5. The aberrant areas are indicated by blue and red rectangles. Dots indicate the positions of the probes and green dots indicate $\log_2$ ratio under −0.5. Physical map corresponding to the highlighted area is depicted below the aCGH data. Rectangles indicate the positions of the UCSC genes (hg18). Colored rectangles indicate the genes included in the overlapped deletion region, and the genes showing high expression in the brain are indicated in red. Italic symbols indicate gene names.

Tzschach et al. [2006] reported on a patient with failure to thrive, psychomotor retardation, and mild facial dysmorphic features who carried a de novo deletion of 5q23.3q31.2, which did not overlap with those of our patients [Tzschach et al., 2006]. Mosca et al. [2007] reported a girl presenting with an abnormal cry, upslanting palpebral fissures, hypertelorism, anteverted nostrils, microretrognathia, growth retardation, and an adenoid cyst at the base of the tongue [Mosca et al., 2007]; the chromosomal deletion in this girl partially overlapped with that in Patient 1 of the present study, but the deletion did not involve the 5q31.3 band (Fig. 5).

In the present study, the common 2.6-Mb deletion region within the chromosomal band 5q31.3 is gene rich, containing 40 genes (UCSC Human genome browser, March 2006; http://genome.ucsc.edu/). The most intriguing finding is that the deleted region contained 5 genes classified as the protocadherin (PCDH) family which can be further divided into two main categories including clustered and non-clustered [Morishita and Yagi, 2007]. The clustered PCDHs including *PCDHA*, *PCDHB*, and *PCDHG*, which

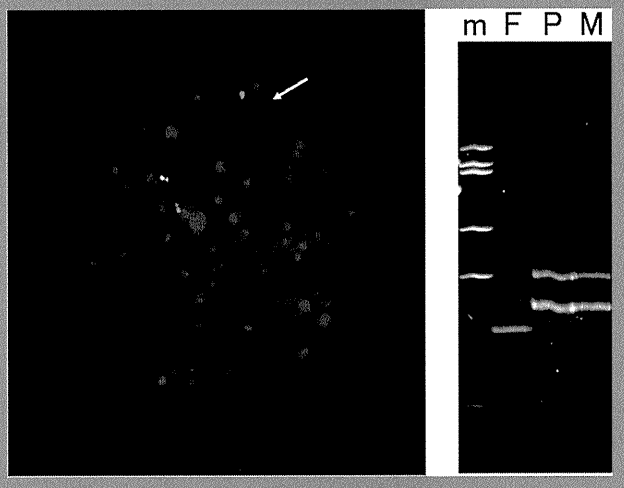

FIG. 4. Molecular cytogenetic validations for Patient 1. Two-color FISH analysis for patient 1 (left) using a combination of the BAC clones RP11-94J21 (red) and RP11-678N8 (green) as probes according to methods described elsewhere. A single green signal indicates the deletion of this region on the chromosome 5 (arrow). Microsatellite marker analysis of D5S1979 (right) separated on a polyacrylamide gel and visualized by staining with ethidium bromide. The bands for this patient are common only with those of the mother. m, molecular size marker; P, patient; F, father; M, mother. BAC clones RP11-94J21 and RP11-678N8 were selected from UCSC Human genome browser build 2006 (http://genome.ucsc.edu/cgi-bin/hgGateway).

are sequentially organized on the 5q31.3 region (Fig. 3) [Yagi, 2008]. The other non-clustered PCDHs, *PCDH1* and *PCDH12*, were also included in this region. PCDHs are highly expressed in the brain where they play roles in directing neurons during brain development, neuronal differentiation, and synaptogenesis [Akins and Biederer, 2006]. Although clustered PCDHs are suspected to have more important roles than non-clustered PCDHs in neuronal development, human diseases that are associated with clustered PCDHs have not yet been reported. The genomic organization of *PCDHA* and *PCDHG* includes multiple variable exons and a set of constant exons, similar to the gene encoding immunoglobulins and T-cell receptors [Morishita and Yagi, 2007; Takeichi, 2007]. These exons are combined by cis-splicing of the mRNA, leading to the production of a large number of isoforms and generating more than 50 transcripts from each gene, with various extracellular domain sequences [Morishita and Yagi, 2007; Takeichi, 2007]. Because of these characteristics, *PCDHA* and *PCDHG* are classified as clustered PCDHs. The expression mechanism of clustered PCDHs is also unique; different mouse neurons were found to express different sets of *Pcdha* and *Pcdhg*, indicating monoallelic gene expression that is unique to the clustered PCDHs [Esumi et al., 2005; Hirayama and Yagi, 2006].

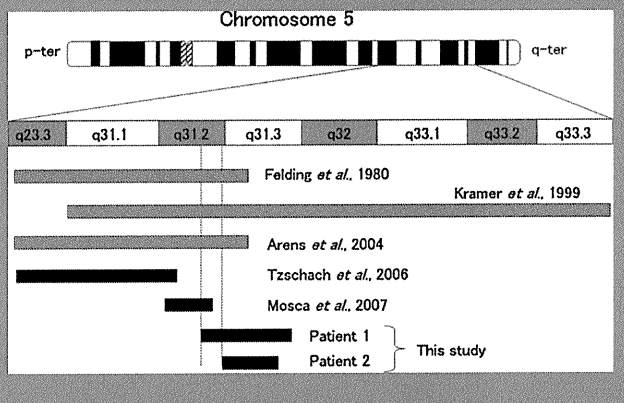

FIG. 5. Physical maps of the 5q31.3 region depict the regions deleted in the previously reported patients. Black rectangles indicate the range of the deletion, and the rectangles with diagonal lines indicate the suspected deletion region based on G-banded karyotyping. The reference author names are also indicated.

Although mutations of human *PCDHA*, *PCDHB*, and *PCDHG* have not been reported, hypomorphic *Pcdha* mutant mice exhibit enhanced contextual fear conditioning and abnormal spatial learning [Fukuda et al., 2008]. Morpholino-based reduction in levels of full-length Pcdh1a protein results in a dramatic increase in the extent of neuronal programmed cell death [Emond and Jontes, 2008]. These observations are similar to those in *Pcdhg−/−* mice that exhibit a loss of spinal interneurons [Wang et al., 2002]. Heterozygous mice of both *Pcdha* and *Pcdhg* have not been reported to show any neurological pathologies [Wang et al., 2002; Fukuda et al., 2008]; however, functional relevance of both *PCDHA* and *PCDHG* to human disorders cannot be denied, because mice heterozygous for the knockout alleles such as *Nsd1* and *Foxc1* show no manifestations [Rayasam et al., 2003; Aldinger et al., 2009]. Hemi-allelic deletions of the human homogues, *NSD1* and *FOXC1*, are associated with human disorders, i.e., Sotos syndrome and Dandy–Walker malformation, respectively. These findings suggest the biological difference between mice and human.

Another study showed that myelination functions as a trigger for the decline in Pcdha expression [Morishita et al., 2004]. Delayed myelination was another characteristic of our patients and may be associated with the deletions of *PCDHA*. Furthermore, *PCDHA* and *PCDHG* exhibit monoallelic expression [Esumi et al., 2005]. Thus, partial monosomy of 5q31.3 may affect the function of *PCDHA* and/or *PCDHG*.

By use of the UCSC genome browser, 6 genes other than *PCDHA* and *PCDHG* were found to be highly expressed in the brain among the 40 genes included in the common deletion region (Supplemental Table SI online). Neuregulin 2 gene (*NRG2*) was one of the 6 genes. *NRG2* is a member of the neuregulin family of signaling proteins that mediate cell–cell interactions in the nervous system and other organs [Rimer, 2007]. Recent genetic, transgenic, and postmortem brain studies support a potential contribution of NRG1-erbB4 signaling in schizophrenia [Banerjee et al., 2010]. Furthermore, *NRG2* is predominantly expressed by neurons in the central nervous system and exerts its effects on the perisynaptic Schwann cells at the neuromuscular junction [Longart et al., 2004; Rimer, 2007], suggesting a possible association of *NRG2* with neurological diseases. The findings of histological examinations of

the brain of *Nrg2* transgenic mice did not differ from those of the wild-type or heterozygous mice; however, homozygous knockout mice showed severe growth retardation, increased morbidity, and reduced reproductive capacity [Britto et al., 2004]. Thus, the peripheral neuropathy in Patient 1 may be attributable to *NRG2* deletion.

In this study, we reported the first two patients with deletions of the 5q31.3 region. We suggest that the deletion of 5q31.3, including clustered PCDHs and *NRG2*, lead to severe developmental delays, distinctive facial features, and delayed myelination. These characteristic manifestations comprise a new recognizable microdeletion syndrome. Although many genes in this region are highly expressed in the brain, the genes that specifically contributed to the unique characteristics of our patients could not be determined, because the crucial functions of the genes involved in the deletion region remain to be elucidated. Further studies need to be conducted to identify the genes that were associated with the characteristic features of our patients. Microcephaly was observed in Patient 1, but the head circumference of Patient 2 was within normal limit. Therefore, the gene associated with microcephaly in Patient 1 might be excluded from the deletion region that was common to both patients.

ACKNOWLEDGMENTS

Dr. Shimojima thanks Hayashi Memorial Foundation for Female Natural Scientists for the grant aid support. We also would like to acknowledge the DECIPHER database for bringing together similar patients from different groups.

REFERENCES

Akins MR, Biederer T. 2006. Cell–cell interactions in synaptogenesis. Curr Opin Neurobiol 16:83–89.

Aldinger KA, Lehmann OJ, Hudgins L, Chizhikov VV, Bassuk AG, Ades LC, Krantz ID, Dobyns WB, Millen KJ. 2009. FOXC1 is required for normal cerebellar development and is a major contributor to chromosome 6p25.3 Dandy–Walker malformation. Nat Genet 41:1037–1042.

Arens YH, Engelen JJ, Govaerts LC, van Ravenswaay CM, Loneus WH, van Lent-Albrechts JC, van der Blij-Philipsen M, Hamers AJ, Schrander-Stumpel CT. 2004. Familial insertion (3;5)(q25.3;q22.1q31.3) with deletion or duplication of chromosome region 5q22.1-5q31.3 in ten unbalanced carriers. Am J Med Genet Part A 130A:128–133.

Banerjee A, Macdonald ML, Borgmann-Winter KE, Hahn CG. 2010. Neuregulin 1-erbB4 pathway in schizophrenia: From genes to an interactome. Brain Res Bull 83:132–139.

Britto JM, Lukehurst S, Weller R, Fraser C, Qiu Y, Hertzog P, Busfield SJ. 2004. Generation and characterization of neuregulin-2-deficient mice. Mol Cell Biol 24:8221–8226.

Emond MR, Jontes JD. 2008. Inhibition of protocadherin-alpha function results in neuronal death in the developing zebrafish. Dev Biol 321:175–187.

Esumi S, Kakazu N, Taguchi Y, Hirayama T, Sasaki A, Hirabayashi T, Koide T, Kitsukawa T, Hamada S, Yagi T. 2005. Monoallelic yet combinatorial expression of variable exons of the protocadherin-alpha gene cluster in single neurons. Nat Genet 37:171–176.

Felding I, Kristoffersson U. 1980. A child with interstitial deletion of chromosome No. 5. Hereditas 93:337–339.

Fukuda E, Hamada S, Hasegawa S, Katori S, Sanbo M, Miyakawa T, Yamamoto T, Yamamoto H, Hirabayashi T, Yagi T. 2008. Down-regulation of protocadherin-alpha A isoforms in mice changes contextual fear conditioning and spatial working memory. Eur J Neurosci 28: 1362–1376.

Garcia-Minaur S, Ramsay J, Grace E, Minns RA, Myles LM, FitzPatrick DR. 2005. Interstitial deletion of the long arm of chromosome 5 in a boy with multiple congenital anomalies and mental retardation: Molecular characterization of the deleted region to 5q22.3q23.3. Am J Med Genet Part A 132A:402–410.

Hirayama T, Yagi T. 2006. The role and expression of the protocadherin-alpha clusters in the CNS. Curr Opin Neurobiol 16:336–342.

Komoike Y, Shimojima K, Liang JS, Fujii H, Maegaki Y, Osawa M, Fujii S, Higashinakagawa T, Yamamoto T. 2010. A functional analysis of GABARAP on 17p13.1 by knockdown zebrafish. J Hum Genet 55:155–162.

Kramer RL, Feldman B, Ebrahim SA, Kasperski SB, Johnson MP, Evans MI. 1999. Molecular cytogenetic analysis of a de novo 5q31q33 deletion associated multiple congenital anomalies: Case report. Am J Med Genet 82:143–145.

Longart M, Liu Y, Karavanova I, Buonanno A. 2004. Neuregulin-2 is developmentally regulated and targeted to dendrites of central neurons. J Comp Neurol 472:156–172.

Morishita H, Kawaguchi M, Murata Y, Seiwa C, Hamada S, Asou H, Yagi T. 2004. Myelination triggers local loss of axonal CNR/protocadherin alpha family protein expression. Eur J Neurosci 20:2843–2847.

Morishita H, Yagi T. 2007. Protocadherin family: Diversity, structure, and function. Curr Opin Cell Biol 19:584–592.

Mosca AL, Callier P, Leheup B, Marle N, Jalloul M, Coffinet L, Feillet F, Valduga M, Jonveaux P, Mugneret F. 2007. Fortuitous FISH diagnosis of an interstitial microdeletion (5)(q31.1q31.2) in a girl suspected to present a cri-du-chat syndrome. Am J Med Genet Part A 143A:1342–1347.

Rayasam GV, Wendling O, Angrand PO, Mark M, Niederreither K, Song L, Lerouge T, Hager GL, Chambon P, Losson R. 2003. NSD1 is essential for early post-implantation development and has a catalytically active SET domain. EMBO J 22:3153–3163.

Rimer M. 2007. Neuregulins at the neuromuscular synapse: Past, present, and future. J Neurosci Res 85:1827–1833.

Takeichi M. 2007. The cadherin superfamily in neuronal connections and interactions. Nat Rev Neurosci 8:11–20.

Tzschach A, Krause-Plonka I, Menzel C, Kalscheuer V, Toennies H, Scherthan H, Knoblauch A, Radke M, Ropers HH, Hoeltzenbein M. 2006. Molecular cytogenetic analysis of a de novo interstitial deletion of 5q23.3q31.2 and its phenotypic consequences. Am J Med Genet Part A 140A:496–502.

Visser R, Matsumoto N. 2003. Genetics of Sotos syndrome. Curr Opin Pediatr 15:598–606.

Wang X, Weiner JA, Levi S, Craig AM, Bradley A, Sanes JR. 2002. Gamma protocadherins are required for survival of spinal interneurons. Neuron 36:843–854.

Yagi T. 2008. Clustered protocadherin family. Dev Growth Differ 50: S131–140.

Acta Neuropathol (2011) 122:775–781
DOI 10.1007/s00401-011-0916-x

CASE REPORT

An autopsy case of adult-onset hereditary spastic paraplegia type 2 with a novel mutation in exon 7 of the proteolipid protein 1 gene

Satoshi O. Suzuki · Toru Iwaki · Kenji Arakawa · Hirokazu Furuya · Naoki Fujii · Akiko Iwaki

Received: 29 September 2011 / Revised: 9 November 2011 / Accepted: 12 November 2011 / Published online: 20 November 2011

Abstract We report an autopsy case of rare adult-onset spastic paraplegia type 2 (SPG2) with a novel missense mutation in exon 7 of the proteolipid protein 1 gene (*PLP1*). The patient was a 67-year-old man whose elder brother had died of a similar disease with onset in his 40s. Thirty-three years before death at the age of 35, he noticed difficulty in walking. He gradually became abasic over a period of 6 years. He also developed progressive dementia and eventually became bed-ridden by 28 years after onset. At autopsy, gross inspection revealed diffuse, moderate atrophy of the cerebrum with a dilated ventricular system and softening of the white matter throughout the central nervous system (CNS). Histopathologically, the CNS showed widespread myelin pallor in the white matter. By contrast, the gray matter and peripheral nerves were well preserved. Some white matter tracts, including the corticospinal tracts, were preferentially affected, and severe axonal degeneration was observed in these tracts. Genetic analysis revealed a novel mutation, p.Tyr263Cys, in exon 7 of *PLP1*. This case represents an adult-onset SPG2 patient with one of the oldest ages of onset reported to date. The late onset and long clinical course suggest that this novel mutation does not affect the maturation of oligodendrocytes, but is related to insufficient maintenance of myelin.

Keywords Proteolipid protein 1 · Gene mutation · Hereditary spastic paraplegia · SPG2 · Adult onset

S. O. Suzuki (✉) · T. Iwaki
Department of Neuropathology,
Graduate School of Medical Sciences,
Kyushu University, Fukuoka 812-8582, Japan
e-mail: sosuzuki@np.med.kyushu-u.ac.jp

K. Arakawa · H. Furuya · N. Fujii
Department of Neurology,
Neuro-Muscular Center,
National Ohmuta Hospital,
Fukuoka 837-0911, Japan

A. Iwaki
Division of Human Molecular Genetics,
Research Center for Genetic Information,
Medical Institute of Bioregulation,
Kyushu University, Fukuoka 812-8582, Japan

Introduction

Spastic paraplegia type 2 (SPG2; MIM#312920) is an X-linked hereditary spastic paraplegia caused by a proteolipid protein 1 gene (*PLP1*) alteration that is allelic to Pelizaeus–Merzbacher disease (PMD; MIM#312080) [3, 20, 25]. Various types of *PLP1* alteration, including entire gene duplications, deletions and point mutations, have been reported, and there is a wide spectrum of clinical manifestations and severities ranging from pure spastic paraplegia to a severe connatal form of PMD with certain genotype–phenotype correlations [1, 14, 20, 25]. SPG2 patients usually develop symptoms in the first decade of life, and adult onset of the disease is very rarely encountered [22]. We herein report an autopsy case of adult-onset SPG2 with a novel Tyr263Cys mutation in PLP1. This case represents an adult-onset SPG2 patient with one of the oldest ages of onset reported to date. The late onset and long clinical course suggest that this novel mutation does not affect the maturation of oligodendrocytes, but is related to the insufficient maintenance of myelin.